Kobe University Repository : Kernel

PDF issue: 2025-12-05

Disproportionation Phenomenon at the Silica Interface of Propylene Carbonate-1,2-Dimethoxyethane Binary Solvent Containing Lithium Perchlorate

Suzuki, Yoshimasa ; Kunikata, Nobuaki ; Kasuya, Motohiro ; Maki, Hideshi ; Matsui, Masaki ; Kurihara, Kazue ; Mizuhata, Minoru

(Citation)
The Journal of Physical Chemistry C,126(28):11810-11821

(Issue Date)
2022-07-12

(Resource Type)
journal article

(Version)
Accepted Manuscript

(Rights)
This document is the Accepted Manuscript version of a Published Work that appeared in final form in The Journal of Physical Chemistry C, copyright © 2022 American Chemical Society after peer review and technical editing by the publisher. To access the final edited and published work see http://pubs.acs.org/articlesonrequest/AOR-…

(URL)
https://hdl.handle.net/20.500.14094/0100477339

KOBE UNIVERSITY

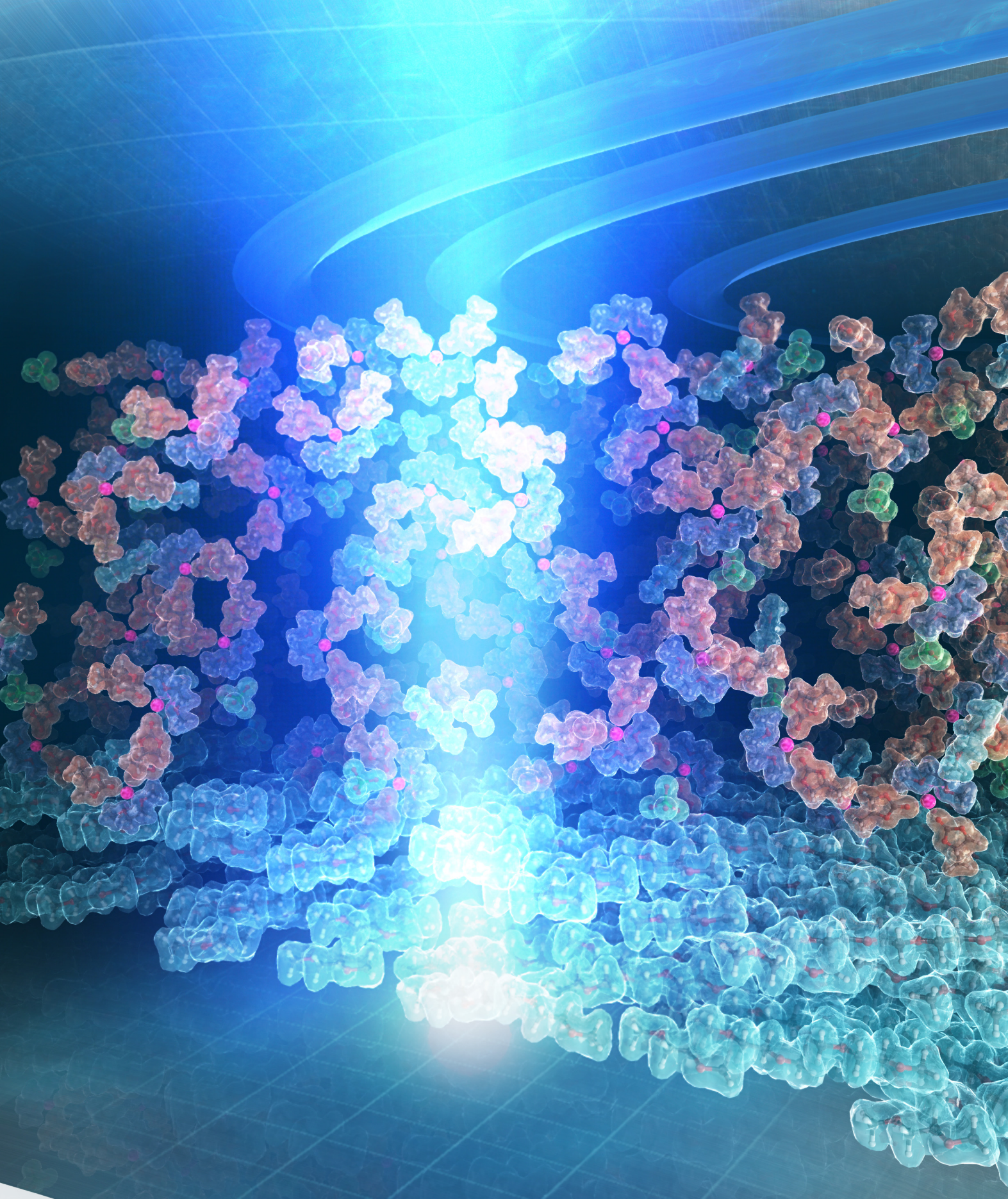

Disproportionation Phenomenon at the Silica Interface of Propylene Carbonate–1,2-Dimethoxyethane Binary Solvent containing Lithium Perchlorate

Yoshimasa Suzuki, [†, ‡] *Nobuaki Kunikata,* [†, ‡, ††] *Motohiro Kasuya,* [¶, ||] *Hideshi Maki,* [†] *Masaki Matsui,* [†, #] *Kazue Kurihara,* [Δ, *] *and Minoru Mizuhata*[†, §, *]

[†]Department of Chemical Science and Engineering, Graduate School of Engineering, Kobe University, 1-1 Rokkodai-cho, Nada, Kobe 657-8501, Japan

[¶]Institute of Multidisciplinary Research for Advanced Materials, Tohoku University, 2-1-1 Katahira, Aoba-ku, Sendai 980-8577, Japan

[||]Faculty of Production Systems Engineering and Sciences, Komatsu University, Nu 1-3 Shicho-machi, Komatsu, Ishikawa 923-8511, Japan

[#]Department of Chemistry, Faculty of Science, Hokkaido University, Kita-10 Nishi-8, Kita, Sapporo 060-0810, Japan

[Δ]New Industry Creation Hatchery Center (NICHe), Tohoku University, 6-6 Aoba, Aramaki, Aoba, Sendai 980-8579, Japan

[§]Faculty of Chemistry, Jagiellonian University, Gronostajowa 2, 30-387 Kraków, Poland

[‡] *Yoshimasa Suzuki and Nobuaki Kunikata contributed equally to this paper*

[††]Present Addresses: Toyama Industrial Technology Research and Development Center, 150, Takaoka, Toyama 933-0981, Japan

KEYWORDS

Micro heterogeneity, Solution structure, Quantitative ^{1}H NMR, Resonance shear measurements

ABSTRACT

Solution structures at solid–liquid interfaces play important roles in electrochemical reaction systems. To gain insights into interactions between binary solutions and metal oxides, we used quantitative ^{1}H NMR and resonance shear measurements to investigate the behavior of a mixed solvent of propylene carbonate (PC)–1,2-dimethoxyethane (DME) at the interface with SiO_2. The PC–DME mixture formed a well-ordered structure at the SiO_2 interface, with the viscosity increasing from 0.5 mPa s in the bulk to 10^5 mPa s at 25 nm from the SiO_2 surface. This long-range structure resulted from the preferential concentration of DME on the SiO_2 surface owing to the different absorptivities of the solvent molecules. $LiClO_4$ addition reduced the distance from the SiO_2 surface at which the solution structure formed to 10 nm at 1.0 mol L^{-1} and 7.5 nm at 2.0 or 3.0 mol L^{-1}. This interfacial structure affected ionic conduction and was consistent with the distance from the SiO_2 surface at which the activation energy of ionic conduction in solid–liquid systems became 10 kJ mol^{-1} greater than the bulk value. The disproportionation of the solvent mixture at the SiO_2 interface was competitive with ion solvation but was suppressed when the $[DME]/[Li^+]$ ratio was ≤ 2.6.

1. INTRODUCTION

In both fundamental and practical electrochemical systems, which often have complex morphologies and geometries, the redox reaction proceeds at a solid–liquid interface. Even in dispersed systems of isolated particles, an electric double layer forms on the surfaces of solids owing to the disproportionation of ions in the liquid phase and the orientation of molecules at the interface. Knowledge about the structure at this solid–liquid interface is very important and has long been of interest for understanding electrochemical reactions.[1–8] In particular, the structure of the electrode interface is involved in solid–electrolyte interphase (SEI) formation[1–6] and charge-transfer resistance.[7,8] According to the Poisson–Boltzmann distribution in which the Gouy–Chapman electric double layer theory is applied as a structural model of a solid–liquid interface,[9,10] counterions, which have the opposite charge to the solid phase surface, concentrate near the solid phase. In this model, ions are point charges and their distribution at the solid–liquid interface is constant, regardless of the ion type. However, model refinements by Stern et al. indicate that the double layer depends on ion size[11] and solvation as well as the dipole interactions of solvent molecules. Among these factors, the effect of differences in the polarity of solvent molecules on the solid–liquid interface structure is of particular interest.

To control ionic conduction, expand electrochemical windows, and improve the stability of species dissolved in electrolyte solutions, binary systems of nonaqueous solvents with significantly different polarities are commonly used as the electrolytes in electrochemical devices.[12–14] We have investigated the influence of such binary systems on the interface structure using a cyclohexane–ethanol mixture. In this binary solvent, a long-distance ethanol layer is adsorbed on the silica surface owing to hydrogen bonding interactions between surface silanol groups and ethanol hydroxyl groups.[15–17] Kitaoka et al, investigated the interfacial liquid structure at the solid interface

of this ethanol-cyclohexane mixture using molecular dynamics simulation and examined the effects of hydrophilicity and hydrophobicity on the solid surface, molecular orientation, size of cluster structure.[18] For electrochemical devices, a solvent combination with a greater polarity difference is typically selected, such as propylene carbonate (PC) and 1,2-dimethoxyethane (DME), which have dielectric constants of 66.8 and 6.92, respectively.[19] We previously found that the electrical conductivity of $LiClO_4$ solutions in a mixture of PC and DME ($LiClO_4$ $PC_{1-x}DME_x$) was maximized at approximately $x = 0.5$ in the bulk. By contrast, in the presence of the metal oxide $LiCoO_2$, the electrical conductivity was maximized at $x = 0$ and decreased monotonically as the DME content increased.[20] Furthermore, in the PC–DME solution, the activation energy of ionic conduction increased at a distance of 100 nm or less from the $LiCoO_2$ surfaces, which was attributed to a change in the solution structure at the solid–liquid interface. However, to clarify the interactions between binary solutions and metal oxides, a more detailed understanding of the solution structures at solid–liquid interfaces is required.

For binary nonaqueous solvents used in electrochemical devices, most studies on the structure at the solid–liquid interface have been carried out using simulation calculations,[21–24] whereas only a few experimental studies have been carried out using spectroscopic and structural techniques such as X-ray reflectivity (XRR)[25] and sum frequency generation spectroscopy (SFG).[26,27] Although XRR can provide information such as the density profile of the solution at the solid–liquid interface, the density profile of each solvent cannot be obtained. Furthermore, using SFG, the abundance ratio of the solvents at the solid–liquid interface can be determined from the relative intensities of the solvent absorption spectra, but no information on distances from the solid–liquid interface can be obtained. By contrast, a more in-depth understanding can potentially be obtained using quantitative ^{1}H NMR (q-^{1}H NMR) spectroscopy and resonance shear measurement (RSM)

based on a surface forces apparatus (SFA).[28,29] Grunberg et al. reported that no peak was detected for water molecules adsorbed on the silica wall surface by static (nonrotating) ^{1}H solid-state NMR.[30] Based on this result, we have investigated the effect of various interactions on the intensity of NMR measurements. We have reported that solvent molecules solvated with ions[31] or interacting with a solid surface[32] or ions in the double layer[33] are not detectable by NMR spectroscopy. Owing to this property, the amounts of PC and DME detected upon SiO_2 addition may provide information about the abundance ratio of solvent molecules at the solid–liquid interface. RSM, which is sensitive to changes in the viscosity of a confined liquid, revealed that the viscosity of water between mica surfaces increases when the surface separation is less than 1 nm,[34] and that the viscosities of $[C_4min][NTf_2]$ and $[C_4min][BF_4]$ increase when the surface separation is less than 10.0 and 6.9 nm, respectively.[35] Such viscosity information can be employed to estimate the distance between the solid–liquid interface and a specific solution structure.

In recent years, attention has been focused on the solution structure at electrode interfaces in high concentration solutions.[36–42] Yamada et al. found that the reductive stability and ultrafast-charging character of lithium-ion batteries were enhanced by a highly concentrated organic electrolyte.[36] Even in aqueous systems, the potential window has been found to expand in high concentration solutions.[37–39] In addition, the electrolyte concentration has been reported to affect the composition, shape, and mechanical properties of the SEI and improve cycling properties.[40–42]

In this study, the structure of a binary nonaqueous solvent ($PC_{1-x}DME_x$) near the surface of a metal oxide (SiO_2) was investigated using q-^{1}H NMR measurements and RSM. In addition, to investigate the structure of high concentration solutions at the electrode interface, we examined the effect of $LiClO_4$ concentration on the structure of the $LiClO_4$ $PC_{1-x}DME_x$ solution at the interface with SiO_2. This work provides important insights into the interactions between binary

solutions and metal oxides as well as the changes in the structure and physical properties of solutions at interfaces, which can be useful in the field of electrochemistry.

2. EXPERIMENTAL

2.1 Materials

Well-dispersed fumed silica consisting of SiO_2 (Nippon Aerosil Co. Ltd.) was dried at 130 °C for 24 h in vacuo and employed as the solid phase. The average SiO_2 particle size was ~20 nm, as determined by scanning electron microscopy (JSM 6335F, JEOL Ltd.), and the specific surface area was 120 m^2 g^{-1}, as obtained by the BET adsorption/desorption method with Nova 2200e (Quantachrome Instruments). Binary PC–DME mixtures (Nacalai Tesque Inc.) with DME molar fractions of 0–0.8 were prepared by mixing thoroughly under dehydration conditions molecular sieve 4A (Nacalai Tesque Inc.). $LiClO_4$ (Kishida Chemical Co.) was dried at 180 °C for 24 h in vacuo and then dissolved in the PC–DME solvent at concentrations of 1.0–3.0 mol L^{-1}. Solid–liquid mixed samples were prepared as described elsewhere.[20] The mixing ratio of the solid and liquid phases were adjusted using the volume fraction. In addition, the length over which the solid phase surface affects the liquid phase was estimated using the apparent average thickness, l, which is defined as follows:

$$l = \frac{W_{\mathrm{liq}}/d_{\mathrm{liq}}}{s_{\mathrm{v}}W_{\mathrm{solid}}} \qquad (1)$$

where W_{liq}, W_{solid}, d_{liq}, and s_{v} are the weight of the liquid phase, weight of the solid phase, density of the liquid phase, and specific surface area of the solid, respectively. The apparent average thickness, l, indicates the distance from the solid phase surface at which the liquid phase is present in the solid–liquid mixed sample. A photograph of one example of a solid-liquid coexistence sample is shown in Figure S1.

2.2 q-^{1}H NMR Measurements

^{1}H NMR spectra were recorded using a Varian INOVA 400 NMR spectrometer with a 9.39 T magnet and a 5 mm switchable broadband (5 mmsw) probe (Varian, Inc.). To avoid mixing the sample with a deuterated solvent, a coaxial NMR tube (516-CC-5, SP Wilmad-LabGlass Co.) was used and the outer tube was filled with deuterium oxide (Euriso-Top). The ^{1}H NMR chemical shifts were determined using deionized double distilled water as a second-order external standard with tetramethylsilane as the first-order standard (0 ppm). All experiments were performed at 25 °C. The quantitative analysis of the ^{1}H NMR spectra was carried out following a previous study,[31–33] as defined in the following equation:

$$\frac{N_{\mathrm{x}}}{N_{\mathrm{sample}}} = 10^{\left[\frac{Rg_{\mathrm{ref}} - Rg_{\mathrm{sample}}}{20}\right]} K \frac{Ns_{\mathrm{ref}} I_{\mathrm{sample}}}{Ns_{\mathrm{sample}} I_{\mathrm{ref}}} \qquad (2)$$

where N is the concentration of the chemical species that gives the NMR signal, Rg is the receiver gain of the NMR spectrometer, Ns is the number of FID scans, and I is the integrated intensity of the NMR signal. The subscripts "ref" and "sample" represent the external standard solution and the sample solution, respectively. K is a specific constant corresponding to the measurement conditions such as the NMR sample tube and NMR spectrometer. This constant is approximately unity when similar NMR sample tubes and the same NMR spectrometer are used.

2.3 Resonance Shear Measurements

To evaluate viscosity, RSM was performed as described previously using the setup shown in Figure S2.[28,29] Sufficiently thin and smooth quartz glass sheets were used as a silica substrate following the procedure of Horn et al.[34,35,43] The root mean square and peak-to-valley roughnesses of the silica surfaces were 0.29 ± 0.11 nm and 2.5 ± 0.8 nm, respectively, as reported previously.[34]

To avoid dissolution of the adhesive by DME, a gold layer of ~40 nm (as a half mirror) was directly deposited on the cylindrical silica surface by vacuum deposition, and then a silica layer of ~2 μm was deposited on the gold layer using an rf magnetron sputtering system (SPV2-TMP-T1-RF1/R, Toei Scientific Industrial Co. Ltd.).[44] For RSM, two silica discs were mounted vertically, and the distance between the substrates (D) was controlled by moving one surface up and down. D was determined by fringes of equal chromatic order (FECO) analysis based on the wavelength of diffracted light.[45,46] For PC solution analysis, RSM was performed by sandwiching a liquid sample of ~30 μL between the upper and lower substrates. For PC–DME and DME solution analyses, to avoid DME evaporation effects, RSM was performed by immersing the entire surfaces of the upper and lower substrates in a liquid sample of ~30 mL. The RSM system was composed of an upper surface unit hung by a pair of vertical leaf springs and a lower surface unit mounted on the horizontal leaf spring of the SFA. The upper unit was connected to a four-sectored piezo tube and oscillated laterally with the sinusoidal input voltage (U_{in}) at various angular frequencies (ω). The deflection of the upper unit detected by a capacitance probe was the output voltage (U_{out}). The relationship between the amplitude ratio, U_{out}/U_{in}, and the variation in ω at various D values represents the viscosity and friction of the confined liquid. To confirm reproducibility, the measurements were repeated twice for all solutions, changing the silica substrate and solution. All measurements were conducted at 25 °C.

2.4 Impedance Measurements

For ac impedance measurements, the closed cell shown in Figure S3 was used to prevent changes in sample composition, and the cell was placed in a glove box under a nitrogen atmosphere to maintain the nonaqueous system. Measurements were performed using an ac four-terminal method

with LCR meters (HP 4284A, Agilent Technologies). To obtain the activation energy of electrical conductivity (ΔE_a), electrical conductivity measurements were carried out in the temperature range of 20–40 °C. The activation energies were calculated as previously reported.[20]

2.5 Raman Spectroscopy Measurements

Raman spectra were recorded using a T-64000 Raman spectrometer (HORIBA, Ltd.) equipped with a Nb: YVO_4 laser and a charge-coupled device cooled using liquid nitrogen as a detector. The 532 nm line was used for excitation. The solid–liquid samples were loaded into glass tubes and spectra were recorded in the back-scattering geometry. The monochromator was calibrated using the silicon peak at 520 cm^{-1}. All experiments were performed at 25 °C.

3. RESULTS AND DISCUSSION

3.1 q-^{1}H NMR and RSM Observations of PC–DME Disproportionation at the SiO_2 Interface

q-^{1}H NMR spectroscopy was used to study solution structures at the interface with a metal oxide. First, to clarify the interactions between the solution and the metal oxide, measurements were performed with a mixed solvent system and SiO_2 without salt addition. Figure 1a–c show the typical ^{1}H NMR spectra of the PC, DME, and $PC_{0.6}DME_{0.4}$ solvent systems in the presence of SiO_2. Peaks corresponding to each ^{1}H nuclei in PC and DME were observed. In bulk PC–DME, one doublet (1.86 ppm), two triplets (4.50 and 5.03 ppm), and one sextet (5.34 ppm) were assigned to the methyl, methylene, and methine groups, respectively, of PC, whereas two singlets (3.75 and 3.94 ppm) were assigned to the methyl and methylene groups, respectively, of DME. The small peak at ~4.88 ppm was derived from H_2O present in the D_2O in the outer tube. With increasing SiO_2 addition, the position shifts toward the lower magnetic field. The shift of the solvent peak

toward the low-field side means that the electron density around each H in the solvent molecules is decreasing, probably because the O atom attracts electrons when the carbonyl group for the PC molecules and the ether group for the DME molecules interact with the SiO_2 surface. As for the line width of the peak, for example, Figure 1(a) shows that for SiO_2/PC, the line width increases with SiO_2 addition from 100 vol% to 60 vol% of liquid phase volume fraction, and decreases with SiO_2 addition below 60 vol% of liquid phase volume fraction. In the 100-60 vol% volume fraction of the liquid phase, the line width of the peak is expected to be wider due to the interaction of solvent molecules with SiO_2, which reduces the mobility, and the exchange of solvent molecules between solvent molecules adsorbed on the SiO_2 surface and solvent molecules in relatively bulk solution away from the solid phase surface, which results in various electron densities. It is considered that when the liquid-phase major fraction is less than 60 vol%, no exchange of solvent molecules occurs between the solvent molecules adsorbed on the solid-phase surface and the relatively bulk solution away from the solid-phase surface. And since the intensity of the peak decreases with the amount of SiO_2 added, the solvent molecules adsorbed on the solid phase surface are not expected to be detected by ^1H NMR. Therefore, the peaks are considered to be narrowed because the solvent molecules appear relatively close to the bulk state. Furthermore, no peaks were detected when the liquid phase volume fraction reached 5 vol% for PC, 7.5 vol% for DME, and 20 vol% for $PC_{0.6}DME_{0.4}$. Typically, in ^1H NMR measurements, the detected amount is proportional to the number of ^1H nuclei. However, the mobility of solvent molecules near a metal oxide surface is limited by interactions with the surface, which reduces the relaxation

time.[31,32] Strong restriction of the movement of solvent molecules near the oxide surface results in the peaks becoming so broad that they cannot be detected. [31-33]

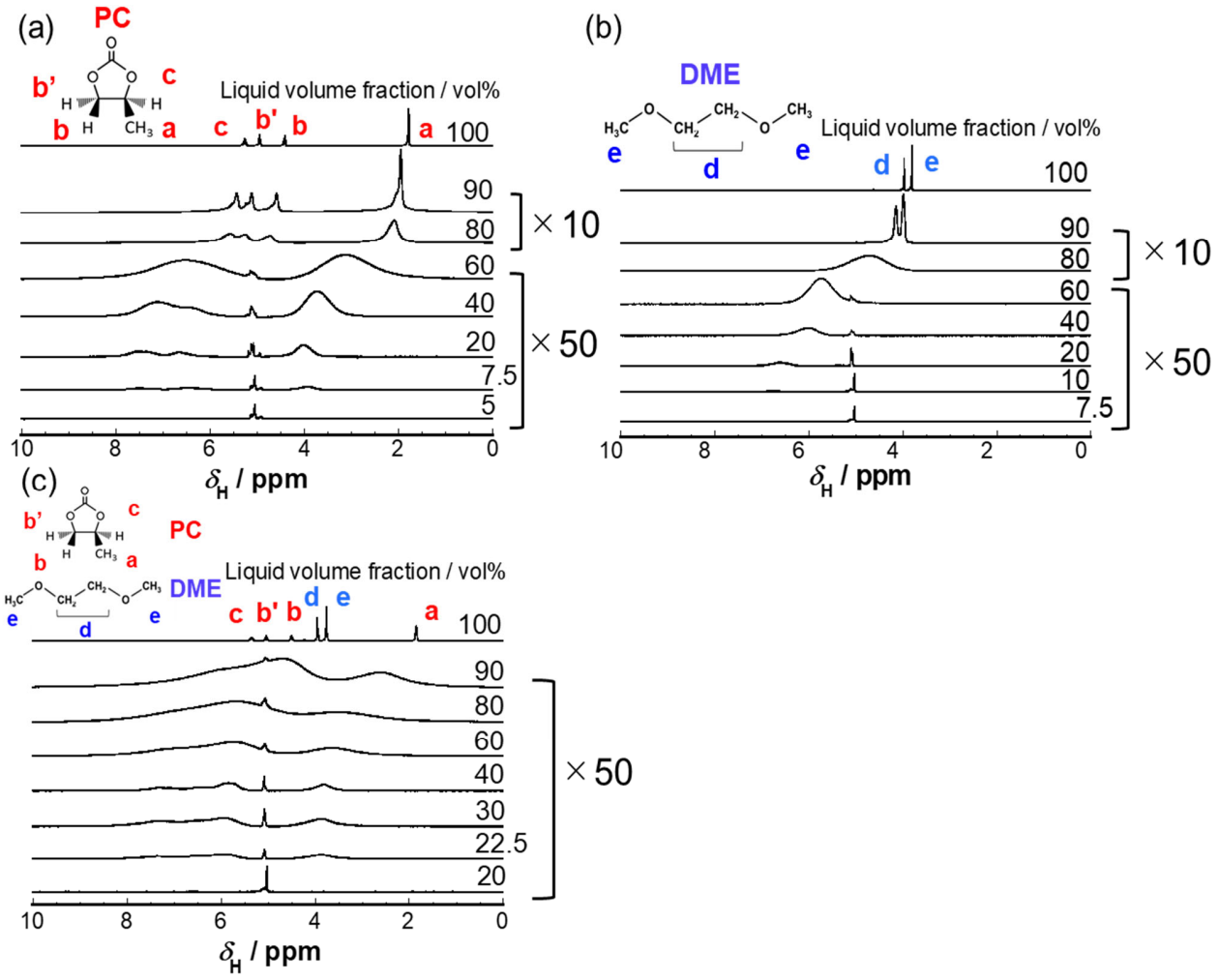

Figure 1. Typical q-^{1}H NMR spectra of solid–liquid systems with various liquid contents: (a) SiO_2/PC, (b) SiO_2/DME, and (c) SiO_2/$PC_{0.6}DME_{0.4}$. To make it easier to identify the peaks, in SiO_2 / PC system, the NMR spectra is multiplied by 10 times for liquid volume fraction with a liquid phase volume fraction of 90,80 vol% and by 50 times for liquid phase volume fraction < 70 vol%. Similarly, in the SiO_2 / DME system, the NMR spectra is multiplied by 10 times for liquid volume fraction with a liquid phase volume fraction of 90,80 vol% and by 50 times for liquid phase volume

fraction < 70 vol%. In $SiO_2/PC_{0.6}DME_{0.4}$ system, the NMR spectrum is multiplied by 50 when the liquid phase volume fraction is less than 90 vol%.

Taking advantage of this property, we investigated the state of the solvent molecules near the SiO_2 surface by quantitatively evaluating the ^1H NMR peaks. Figure 2a–c show the relationship between the liquid phase volume fraction in the PC, DME, and $PC_{0.6}DME_{0.4}$ systems with SiO_2 and the amount of each solvent molecule detected by ^1H NMR spectroscopy.

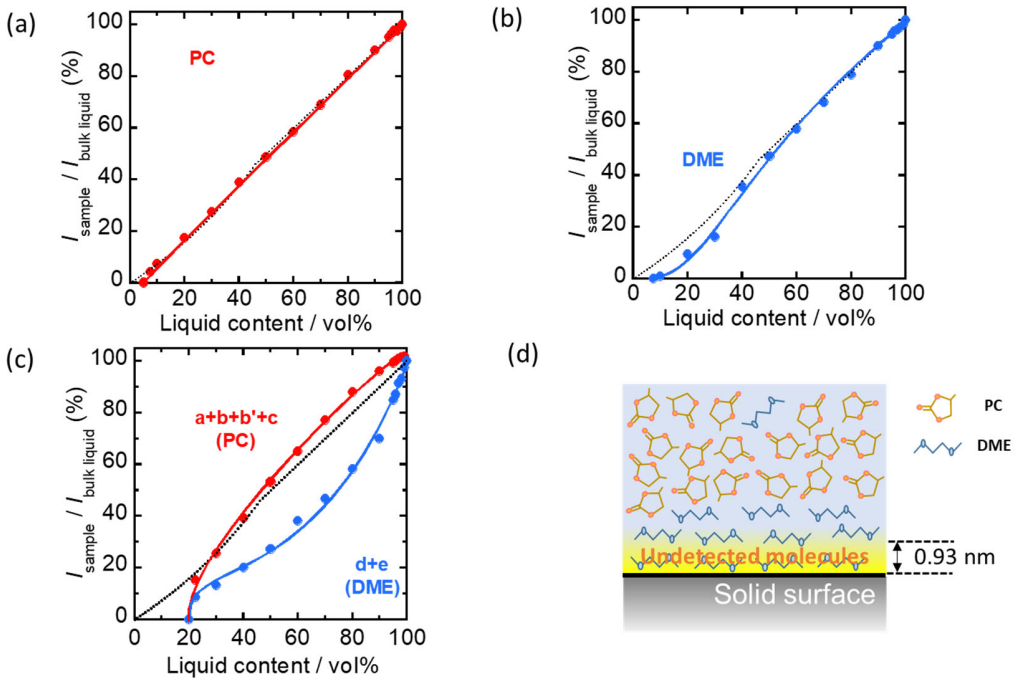

Figure 2. Liquid content dependences of the q-^1H NMR detection ratios of PC (red) and DME (blue) for (a) SiO_2/PC, (b) SiO_2/DME, and (c) $SiO_2/PC_{0.6}DME_{0.4}$. The vertical axis ($I_{sample}/I_{bulk\ liquid}$) represents the detection ratio of each molecule in the liquid phase, as determined by the integrated peak intensity of the solid–liquid sample (I_{sample}) divided by the integrated peak intensity of the bulk liquid ($I_{bulk\ liquid}$). Broken lines represent the expected amounts of PC and DME after adjustment for

the liquid content. For samples with a liquid phase volume fraction of 45.8 vol% or less, the broken lines bend due to the pore volume taken into consideration and calculated from the ratio of the tap density to the true density. Details are indicated in Figure S4. (d) Schematic diagram of the interface for SiO_2 $PC_{0.6}DME_{0.4}$ (Liquid content: 60 vol%). See SI for the calculation of the thickness of the DME layer not detected by ^{1}H NMR.

In the case that SiO_2 was added to pure PC and DME, the detected amounts were slightly below the broken lines (Figure 2a, b). However, when SiO_2 was added to $PC_{0.6}DME_{0.4}$, the detected amount of DME was significantly reduced compared to that of PC. When the liquid phase volume fraction was 30 vol% or more, the detected amount of PC exceeded the broken line. These observations indicate that for $PC_{0.6}DME_{0.4}$ coexisting with SiO_2, the solvent mixture is disproportionated such that DME is concentrated near the SiO_2 surface and PC is located away from the SiO_2 surface, as shown in Figure 2d. In addition, for $PC_{0.6}DME_{0.4}$, the solvent peak is no longer detected when the liquid phase volume fraction is 20 vol%, and the liquid phase volume fraction at which no peaks were detected was higher than that for each pure solvent, indicating that the interactions between the SiO_2 surface and the solvent molecules act over a longer distance in the binary solution. The thickness of the DME layer undetectable by NMR measurement was calculated by the method described in Supporting Information. As shown in Figure 2(d), for example, the DME layer at a distance of 0.93 nm from the SiO_2 surface was undetectable when the liquid phase volume fraction was 60 vol%.

The q-^{1}H NMR results suggest that the mobility of the solvent molecules near the SiO_2 surface is reduced by interactions with the metal oxide surface. Therefore, we measured the shear viscosity of a solution sandwiched between SiO_2 substrates to investigate the viscosity of the solution near

the SiO_2 surface by RSM technique. The resonance curves of $PC_{0.6}DME_{0.4}$ confined between sputtered silica surfaces at various surface separations are shown as Figure 3.

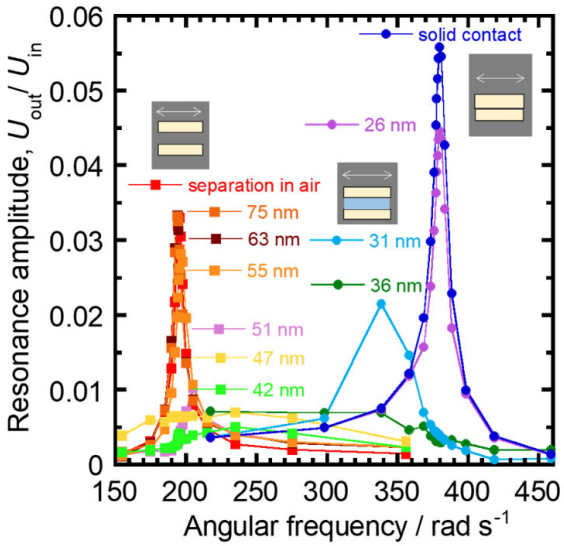

Figure 3. Resonance curves of $PC_{0.6}DME_{0.4}$ confined between sputtered silica surfaces at various surface separations by resonance shear measurement (RSM) technique. The curves for separation in air and solid contact are also plotted as references.

For reference, the curves for separation in air (AS) and solid contact (CS) are also plotted. For $PC_{0.6}DME_{0.4}$, the resonance curve at D = 75 nm exhibited a peak at a resonant frequency (ω_{res}) of 195 rad s^{-1}, which is the same as the frequency for AS. As the distance between the substrates was reduced to D = 55 nm, the peak intensity decreased. When D was further reduced, the peak at ω_{res} = 195 rad s^{-1} disappeared, which indicated that the vibration of the substrate was hindered by the solution. Thus, at D < 55 nm, the shear viscosity of the solution is considered to increase.

Furthermore, at D = 32 nm, a new peak appeared at a higher frequency. Finally, at D = 26 nm, the frequency of the peak matches that for CS. Thus, at D < 26 nm, the upper and lower substrates oscillate at the same time and the motility of the solvent molecules is significantly restricted, which suggests the formation of a large cluster-like structure.

Based on a basic physical model, we calculated an effective viscosity of the solution at each D. Figure 4a shows the mechanical model used for this analysis. In this model, b_1 and b_3 are the damping parameters of the upper and lower units, m_1 and m_2 are masses of the upper and lower units, and k_1 and k_3 are the spring constants of the upper and lower units. For the sample, b_2 is the viscous parameter and k_2 is the elastic parameter.[35] As the sample is a solution, k_2 was regarded as 0. First, we determined the constants for the upper unit from the resonance curve of AS. In the AS state, only the upper unit vibrates, and b_1, k_1, and m_1 contribute to the resonance curve. Therefore, the theoretical resonance curve of the AS peak derived from the corresponding equation of motion can be written as:[28,35]

$$\frac{U_{\text{out}}}{U_{\text{in}}} = \frac{C}{m_1} \frac{1}{\sqrt{(\frac{1}{\alpha}\frac{k_1}{m_1} - \omega^2)^2 + (\frac{b_1}{m_1})^2\omega^2}} \quad (3)$$

where C is an apparatus constant and α is a parameter related to the lateral movement of the upper unit with respect to the movement of the end of the vertical leaf spring. Each constant was obtained by fitting the resonance curve of AS with this equation. The other resonance curves are described by the following equation:[28,35]

$$\frac{U_{\text{out}}}{U_{\text{in}}} = \frac{C}{\alpha}\sqrt{\frac{(K_2 - m_2\omega^2)^2 + \omega^2 B_2^2}{[(K_1 - m_1\omega^2)K_2 - \omega^2 B_1 B_2 - k_2^2 + b_2^2\omega^2]^2 + \omega^2[(K_1 - m_1\omega^2)B_2 + (K_2 - m_2\omega^2)B_1 - 2k_2 b_2]^2}} \quad (4)$$

where $B_1 = b_1 + b_2$, $B_2 = b_2 + b_3$, $K_1 = k_1/\alpha + k_2$, and $K_2 = k_2 + k_3$. The constants for the lower unit was determined from the resonance curve of CS. In this case, the b_2 and k_2 parameters of the sample were removed, and b_3, k_3, and m_2 were obtained by fitting with Eq. (4) using the b_1, k_1, and m_1

values determined from the resonance curve of AS. The b_2 at each D value was obtained by fitting the resonance curves of the sample sandwiched between the SiO_2 substrates at each D value using Eq. (4). Subsequently, the effective viscosity was calculated using $\eta_{eff} = b_2 D/A_{eff}$. Here, the effective area (A_{eff}) was determined to be the bulk viscosity of each solution when D was sufficiently large.[35] Figure 4b shows the effective viscosity dependence of D in pure PC, pure DME, and $PC_{0.6}DME_{0.4}$. In both pure solvents, the effective viscosity was almost constant up to D = 15 nm. However, at lower D values, the effective viscosity increased sharply as D decreased, becoming almost 4 orders of magnitude higher than that of the bulk solvent. By contrast, in $PC_{0.6}DME_{0.4}$, the viscosity began to increase at D = 60 nm, becoming approximately 5 orders of magnitude higher than that of the bulk solvent at D = 30 nm. Considering the q-^{1}H NMR results, disproportionation of the solvent mixture by DME concentration on the SiO_2 surface is considered to increase the distance at which the effective viscosity increases. The disproportionation of the solvent mixture suppresses the exchange of the solvent molecules concentrated on the SiO_2 surface with those in the bulk, resulting in an increase in the effective viscosity.

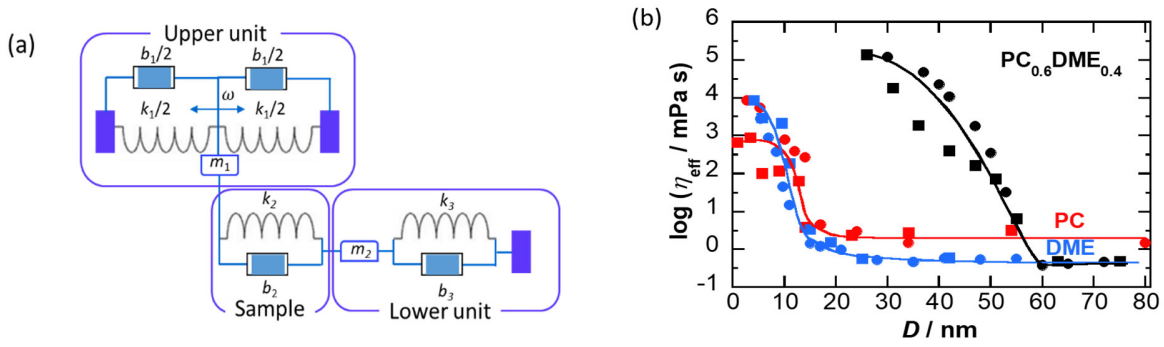

Figure 4. (a) Mechanical model used for RSM analysis. (b) Effective viscosity dependence on D in pure PC, pure DME, and $PC_{0.6}DME_{0.4}$. Different symbols with the same color in each system distinguish the results of measurements made twice to check reproducibility.

3.2 Effect of PC–DME Disproportionation at the SiO_2 Interface on the Electrical Conductivity of $LiClO_4$ $PC_{1-x}DME_x$

The q-^{1}H NMR and RSM results indicated that the PC–DME solvent mixture underwent disproportionation at the SiO_2 interface. We have previously discovered that in the coexistence of $LiCoO_2$ and Al_2O_3 with 1.0 mol L^{-1} $LiClO_4$ $PC_{1-x}DME_x$, the DME content, which has the highest electrical conductivity, is different from that of bulk solvents.[20,47] Therefore, the electrical conductivity of the $LiClO_4$ $PC_{1-x}DME_x$ solution was measured in the presence of SiO_2, and the effect of the nonuniformity of the solvent composition at the solid–liquid interface on the ionic conduction was investigated. Figure 5 shows the dependence of the electrical conductivity on the DME content for SiO_2/1.0 mol L^{-1} $LiClO_4$ $PC_{1-x}DME_x$ at various liquid phase volume fractions.

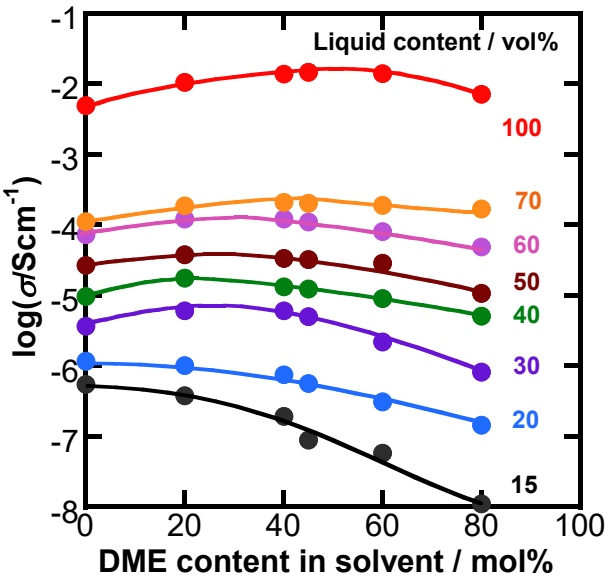

Figure 5. (a)Variation in electrical conductivity with solvent composition and liquid content for SiO_2/1.0 mol L^{-1} $LiClO_4$ $PC_{1-x}DME_x$ at 25 °C.

As shown in Figure 5, in the bulk, the maximum electrical conductivity was observed for the solution with an approximate DME content of x = 0.5, which is consistent with previous reports.[19,48,49] However, when SiO_2 was added, the maximum electrical conductivity was observed at a lower DME content. When the liquid phase volume fraction was 20 vol% or less, the electrical conductivity decreased monotonically as the DME content increased. The same tendency has been observed with $LiCoO_2$ or Al_2O_3 as the solid phase.[20,47]

In the bulk, as the content of DME increased, the viscosity of the solution decreased, resulting in a decrease in the activation energy of ionic conduction as shown in Figure 6a. By contrast, in samples with a liquid phase volume fraction of 50 vol% or less (apparent average thickness of ≤3.8 nm), the activation energy of ionic conduction increased as the DME content increased. This behavior occurs because DME loses fluidity on the SiO_2 surface, which inhibits the ionic conduction. As shown in Figure 6b, the activation energy of ionic conduction increased for samples with a small apparent average thickness. The thickness at which the activation energy of ionic conduction increased was larger than the thickness typically assumed for the electric double layer, suggesting that the viscosity of the solvent molecules is increased by interactions with the SiO_2 surface, which increases the activation energy.

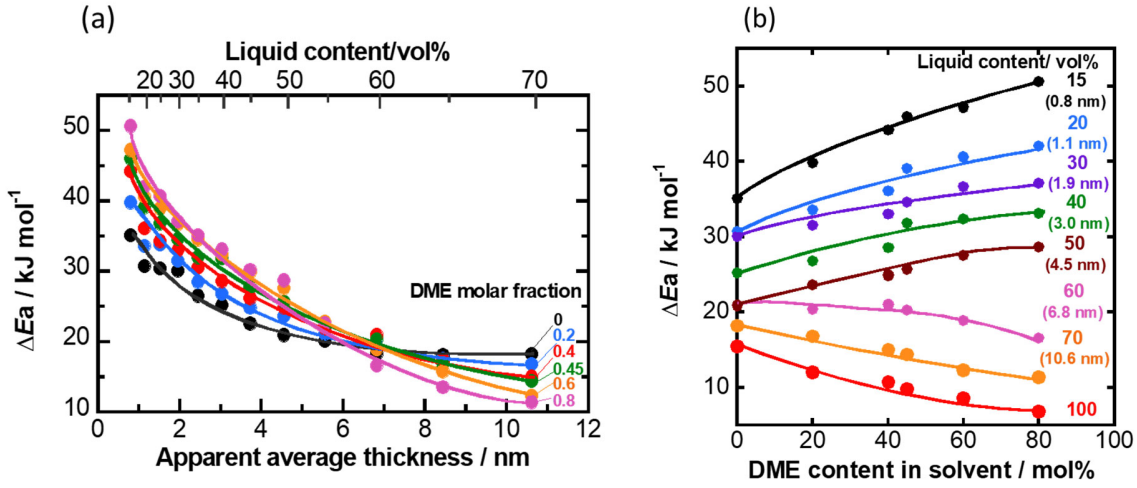

Figure 6. Variations in activation energy with (a) apparent average thickness and (b) DME content for SiO_2/1.0 mol L^{-1} $LiClO_4$ $PC_{1-x}DME_x$.

The thickness at which the activation energy increased became larger as the DME content increased. These observations, which are consistent with the q-^{1}H NMR and RSM results, confirm that the interaction between the SiO_2 surface and the solvent molecules acts over a longer distance in the binary solution. Thus, by investigating the solution structure at the solid–liquid interface, we clarified the origin of the change in the solvent composition dependence of the electrical conductivity for 1.0 mol L^{-1} $LiClO_4$ $PC_{1-x}DME_x$.

3.3 Influence of $LiClO_4$ Concentration on PC–DME Disproportionation at the SiO_2 Interface

To understand how the formation of solvation structures affects the disproportionation of the solvent near the solid–liquid interface and the viscosity reduction effect, the concentration dependence of solvent disproportionation at the SiO_2 surface was investigated. The $LiClO_4$ concentration dependence was investigated using q-^{1}H NMR measurements of $LiClO_4$

$PC_{0.6}DME_{0.4}$ solutions in the presence of SiO_2. At 1.0 mol L^{-1} $LiClO_4$, the addition of SiO_2 caused the detected amount of DME to decrease relative to the amount of PC (Figure 7a). However, the difference in the detected amounts of PC and DME became smaller as the $LiClO_4$ concentration increased. Furthermore, the liquid phase content at which no peak was detected also decreased as the $LiClO_4$ concentration increased. Thus, as the $LiClO_4$ concentration increased, the distance at which the interaction between the SiO_2 surface and the solvent molecules acted decreased, and the concentration of DME on the SiO_2 surface also decreased (Figure 7b). At 3.0 mol L^{-1} $LiClO_4$, the decrease in the detected amounts of PC and DME upon SiO_2 addition was similar (Figure 7c), and disproportionation of the solvent mixture on the SiO_2 surface did not occur (Figure 7d). The liquid phase content at which no peak was detected was also minimized. Based on the apparent average thickness, the solvent molecules that are not detected by ^1H NMR are those at distances of 0.7 nm from the SiO_2 surface for 1.0 mol L^{-1} and 0.4 nm for 3.0 mol L^{-1}. These results indicate that in highly concentrated solutions, the number of solvent molecules interacting with the SiO_2 surface decreases and no disproportionation of the solvent mixture occurs.

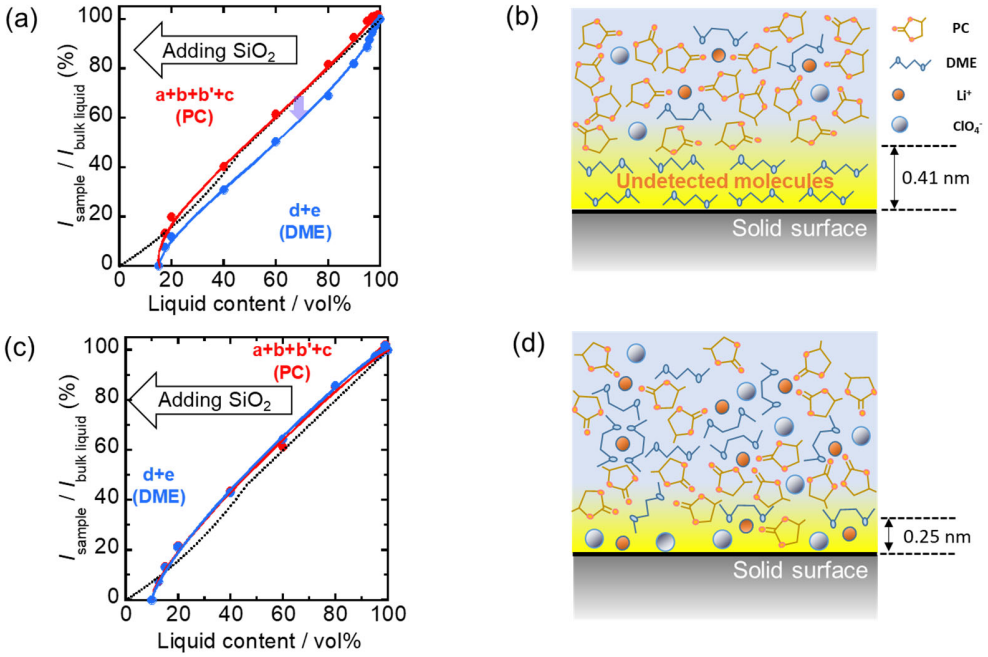

Figure 7. (a,c) Liquid content dependences of the q-^{1}H NMR detection ratios of PC (red) and DME (blue) and (b,d) schematic diagrams of the solid–liquid interface for (a,b) 1.0 mol L^{-1} $LiClO_4$ $PC_{0.6}DME_{0.4}/SiO_2$ (Liquid content: 60 vol%) and (c,d) 3.0 mol L^{-1} $LiClO_4$ $PC_{0.6}DME_{0.4}/SiO_2$ (Liquid content: 60 vol%). See SI for the calculation of the thickness not detected by ^{1}H NMR.

The RSM results also revealed a $LiClO_4$ concentration dependence. Figure 8 shows the effective viscosity dependence of D for PC and $PC_{0.6}DME_{0.4}$ solutions with $LiClO_4$ concentrations of 1.0–3.0 mol L^{-1}. In the PC solutions, the effective viscosity sharply increased at D = 15 nm at all $LiClO_4$ concentrations. By contrast, in the $PC_{0.6}DME_{0.4}$ solutions, the D value at which the effective viscosity increases showed a dependence on the $LiClO_4$ concentration, with the D becoming smaller as the $LiClO_4$ concentration increased. As the distance at which the shear viscosity increased is larger than the thickness of the electric double layer and no concentration dependence was observed in the PC solution, the conventional double layer model cannot explain these results. Thus, the suppression of solvent mixture disproportionation on the SiO_2 surface is considered to result in a decrease in the distance at which the shear viscosity increases.

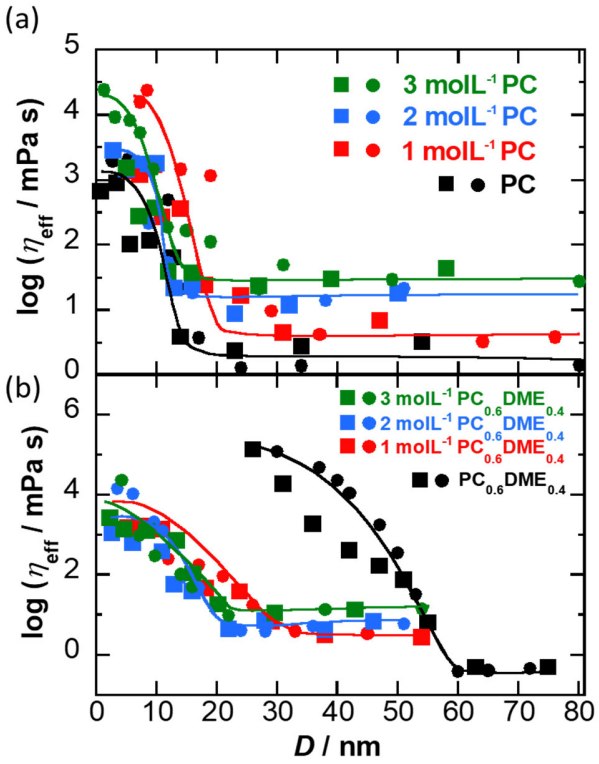

Figure 8. Dependence of effective viscosity on D in (a) 1.0–3.0 mol L^{-1} $LiClO_4$ PC and (b) 1.0–3.0 mol L^{-1} $LiClO_4$ $PC_{0.6}DME_{0.4}$. Different symbols with the same color in each system distinguish the results of measurements made twice to check reproducibility.

In highly concentrated solutions (≥1.0 mol L^{-1} $LiClO_4$), the electrical conductivity increased with the addition of DME, even in solid–liquid systems (liquid phase volume fraction of 15 vol%). In particular, at 3.0 mol L^{-1} $LiClO_4$, the addition of DME resulted in a monotonous increase in the electrical conductivity (Figure 9a). The apparent average thickness at which the activation energy of ionic conduction increased showed no dependence on the DME content, and the activation energy itself decreased with the addition of DME in the solid–liquid systems and in the bulk (Figure 9b). Thus, the viscosity of the solution decreases upon DME addition, even in solid–liquid system with highly concentrated solutions.

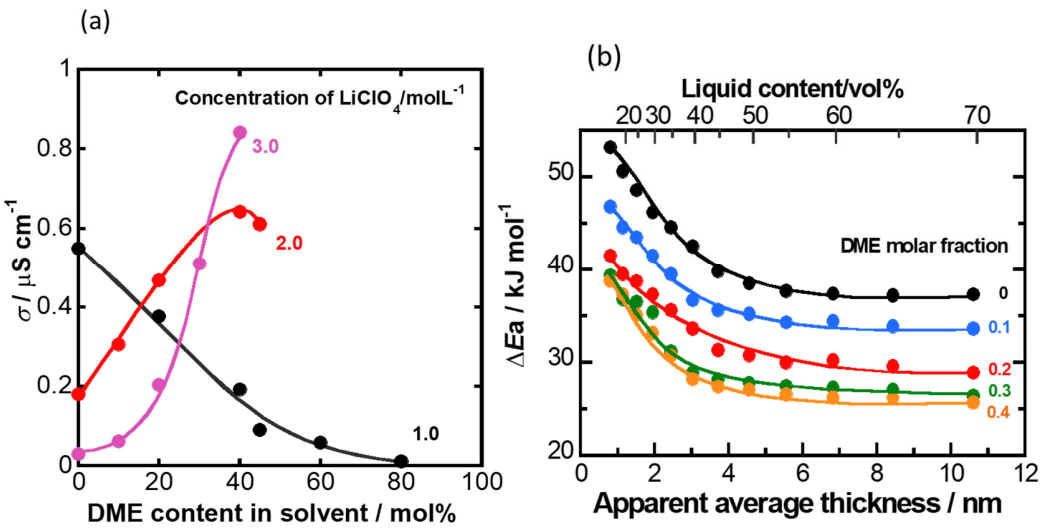

Figure 9. (a) Variation in electrical conductivity with DME content for SiO_2/1.0–3.0 mol L^{-1} $LiClO_4$ $PC_{1-x}DME_x$ (liquid content of 15 vol%) at 25 °C. (b) Variation in activation energy with DME content and apparent average thickness for SiO_2/3.0 mol L^{-1} $LiClO_4$ $PC_{1-x}DME_x$.

Figure 10 shows the apparent average thickness dependence of the activation energy of ion conduction for PC and $PC_{0.6}DME_{0.4}$ solutions with $LiClO_4$ concentrations of 1.0–3.0 mol L^{-1}. The average thickness at which the activation energy increased did not depend on the $LiClO_4$ concentration in PC, whereas a decrease in this value was observed as the $LiClO_4$ concentration increased in $PC_{0.6}DME_{0.4}$. In addition, the apparent average thickness dependence of the activation energy of ion conduction was similar to the distance from the substrate at which the viscosity increased ($D/2$; as D is the distance between the substrates, the distance from the substrate is $D/2$), as shown in Figure 8.

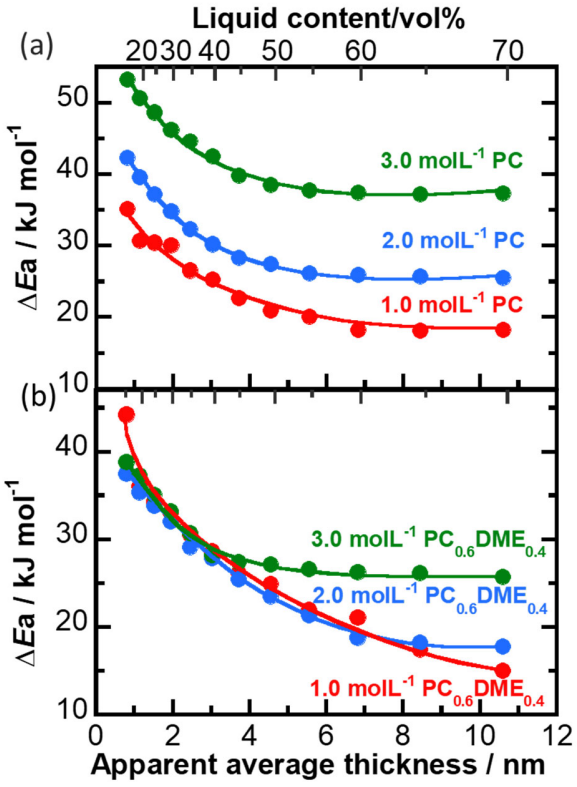

Figure 10. Variations in activation energy with apparent average thickness for (a) SiO_2/1.0–3.0 mol L^{-1} $LiClO_4$ PC and (b) SiO_2/1.0–3.0 mol L^{-1} $LiClO_4$ $PC_{0.6}DME_{0.4}$.

3.4 Solvation Structure of $LiClO_4$ PC–DME Solution in the Presence of SiO_2

We reasoned that DME solvation suppressed the disproportionation of the solvent mixture on the SiO_2 surface in high concentration solutions. Therefore, the solvation structure of the $LiClO_4$ PC–DME solution in the presence of SiO_2 was investigated using Raman spectroscopy. In pure PC, the vibration peak of the symmetric ring deformation band appears near 710 cm^{-1},[50,51] and waveform separation gave peaks at 707 and 714 cm^{-1}. The peak at 707 cm^{-1} was assigned to free PC (I_1) without interactions and the peak at 714 cm^{-1} was attributed to PC (I_2) with intermolecular interactions. Upon SiO_2 addition, a new peak appeared at 730 cm^{-1}, which was attributed to PC interacting with the SiO_2 surface (Figure S9a). Similar to previous reports,[50,51] the $LiClO_4$ PC solution also showed a peak near 730 cm^{-1}, which was not observed for pure PC alone, and this peak was assigned to a PC molecule solvated with Li^+. As the peaks corresponding to PC interacting with the SiO_2 surface and PC solvated with Li^+ appeared similar wavenumbers, only three peaks were observed when SiO_2 was added to the $LiClO_4$ PC solution. Therefore, the I_3 peak was considered to correspond to both PC interacting with the SiO_2 surface and PC solvated with Li^+ (Figure S9a).

For DME, we focused on the stretching vibration peak of C–O–C near 1025 cm^{-1}.[52,53] Pure DME exhibited a single peak (I_4) at 1025 cm^{-1} (Figure S9b). As DME has a smaller permittivity than PC, the intermolecular interactions are weak. Therefore, intermolecular interactions did not affect the position of the observed peak. When SiO_2 was added to DME, no new peak appeared. However, in the $LiClO_4$ DME solution, a peak appeared near 1017 cm^{-1}, which was assigned to DME solvated with Li^+ (I_5; Figure S9b). As no new peak appeared upon SiO_2 addition, the solvation number of DME was calculated using the following equation:

$$\text{DME solvation number} = \frac{I_5}{I_4 + I_5} \frac{[\text{DME}]}{[\text{Li}^+]} \qquad (5)$$

Figure 11 shows the dependence of the relative intensity of I_3 on the DME content for SiO_2/1.0 mol L^{-1} $LiClO_4$ $PC_{1-x}DME_x$. In the bulk solution, I_3 decreased as the content of DME increased, indicating that PC desolvation proceeded. When SiO_2 was added, I_3 increased, which suggests that PC desolvation was suppressed or PC was adsorbed on the SiO_2 surface.

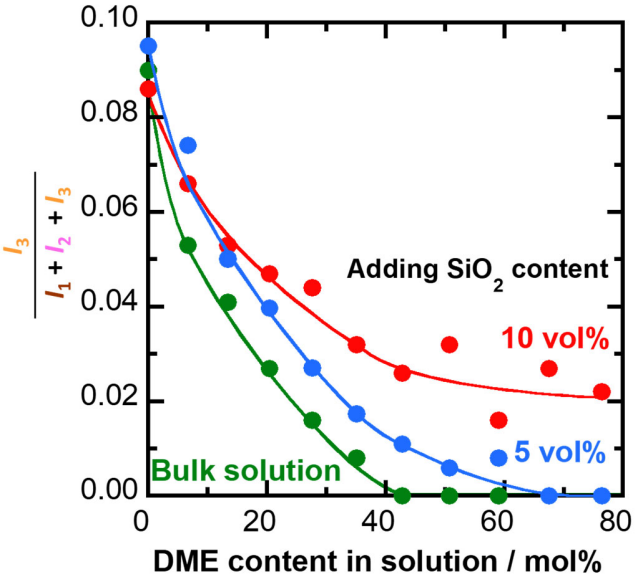

Figure 11. Dependence of the relative intensity of I_3 on the DME content for SiO_2/1.0 mol L^{-1} $LiClO_4$ $PC_{1-x}DME_x$ at various liquid contents. I_1 is assigned to free PC without interactions (707 cm^{-1}). I_2 is assigned to PC with intermolecular interactions (714 cm^{-1}). I_3 is assigned to PC interacting with the SiO_2 surface and PC solvated with Li^+ (730 cm^{-1}).

The dependences of the relative intensity of I_5 and the solvation number of DME on the DME content are shown in Figure 12 for SiO_2/1.0 mol L^{-1} $LiClO_4$ $PC_{1-x}DME_x$. As the content of DME increased, the solvation number of DME increased, which, considering the results for PC, indicates that DME is preferentially solvated by Li^+ in the bulk. There has been discussion of selective solvation of PC and DME with respect to Li^+, with conductivity and Raman spectroscopy

measurements reporting preferential orientation of DME,[48,54-56] and electrospray ionization mass spectrometry reporting co-solvation of PC and DME.[57] On the other hand, MD simulation results report preferential solvation of PC.[58,59] It is unclear why this difference occurs, but in this measurement, the number of donors is 24 for DME and 15 for PC,[60] with DME having a larger number of donors, resulting in preferential solvation of Li^+ with DME in bulk. In the solid–liquid systems, the solvation number of DME was found to be smaller than that in the bulk for solutions containing large amounts of DME. Thus, desolvation of Li^+ from DME and solvation of PC with Li^+ were considered to occur because DME was concentrated on the SiO_2 surface. However, SiO_2 addition did not change the solvation number of DME in solutions with low DME contents, indicating that the desolvation of Li^+ from DME did not occur. Therefore, the concentration of DME on the SiO_2 surface competes with solvation by Li^+. In solutions with [DME]/[Li^+] ratios of ≥3.5, concentration on the SiO_2 surface is favored, whereas in solutions with [DME]/[Li^+] ratios of ≤2.6, solvation by Li^+ is favored. Therefore, increasing the $LiClO_4$ concentration is considered to suppress the concentration of DME on the SiO_2 surface. A discussion of Raman data for PC-DME without $LiClO_4$ is provided in Supporting Information. (Figure S10)

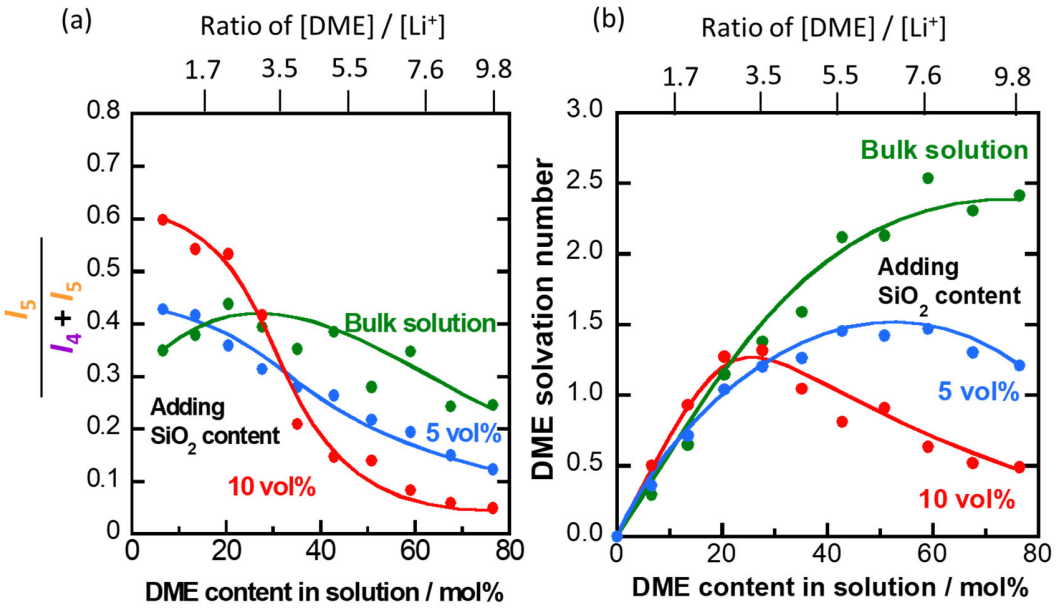

Figure 12. Dependences of (a) the relative intensity of I_5 and (b) the solvation number of DME on DME content for SiO_2/1.0 mol L^{-1} $LiClO_4$ $PC_{1-x}DME_x$. I_4 is assigned to free DME (1025 cm^{-1}). I_5 is assigned to DME solvated with Li^+ (1017 cm^{-1}).

Finally, we discuss the distance at which the SiO_2 surface can interact with solvent molecules. In 1.0 mol L^{-1} $LiClO_4$ $PC_{0.6}DME_{0.4}$, at distances less than 0.7 nm from the SiO_2 surface, the mobility of the solvent molecules is significantly restricted and these molecules are not detected by NMR. At distances less than 10 nm, the viscosity increases and the solvation structure changes. Therefore, in this region, ionic conduction is suppressed and the activation energy increases. At longer distances, the physical characteristics of the solution do not appear to change, and the solvent molecules are considered to have no interactions with the SiO_2 surface. Notably, 10 nm is much larger than the thickness of the electric double layer, and this interaction distance is much longer than estimated by simulation calculations.[21–24] However, this distance depends on the composition and concentration of the solution. For example, lower DME contents and the higher $LiClO_4$ concentrations decrease the distance, and thus phase separation increases the distance.

4. CONCLUSIONS

In this study q-^{1}H NMR measurements and RSM provided insights into the changes in the solution physical properties at solid–liquid interfaces, which are usually difficult to observe. The mobility of solvent molecules near the SiO_2 surface was decreased by interactions with the surface. Furthermore, in PC–DME solutions, DME molecules interacted preferentially with the SiO_2 surface. Similarly, DME was preferentially solvated by Li^+ in $LiClO_4$ PC–DME solutions. The preferential interaction of DME with the SiO_2 surface caused local disproportionation of the solvent mixture, resulting in an increase in viscosity. In addition, the local viscosity of PC–DME solutions increased at a greater distance from the solid surface than those of pure PC and DME because the phase separation of the solution suppressed the exchange of solvent molecules on the surface of the metal oxide with those in the bulk.

As the local viscosity increased, the ionic conductivity of 1.0 mol L^{-1} $LiClO_4$ PC–DME in the presence of SiO_2 became inferior to that of 1.0 mol L^{-1} $LiClO_4$ PC in the presence of SiO_2. Interestingly, this disproportionation phenomenon was influenced by the concentration of ionic species in solution. Moreover, competition occurred between solvation by Li^+ and concentration of DME on the SiO_2 surface. Therefore, at large [DME]/[Li^+] ratios, DME molecules were concentrated on the SiO_2 surface and phase separation occurred, whereas at small ratios, DME molecules were coordinated to Li^+ instead of being concentrated on the SiO_2 surface and no phase separation occurred. Therefore, the distance from the SiO_2 surface at which the viscosity increased in the PC–DME solution decreased with increasing $LiClO_4$ concentration, despite this distance showing no concentration dependence in pure PC. These results clearly demonstrate that the disproportionation of the solvent mixture near the SiO_2 surface is associated with the formation of a highly viscous solution layer over fairly long distances. Because formation of the high-viscosity

solution layer over long distances was suppressed, the electrical conductivity of 3.0 mol L^{-1} $LiClO_4$ $PC_{0.6}DME_{0.4}$ in the presence of SiO_2 was 0.84 μScm^{-1}, which is larger than the conductivity of 3.0 mol L^{-1} $LiClO_4$ PC, 0.33 μScm^{-1}, consistent with the physical properties observed in the bulk solution. Thus, disproportionation of the mixed PC–DME solvent on the SiO_2 surface was shown to cause unexpected changes in the physical properties of the solution. Moreover, the concentration of DME on the SiO_2 surface and solvation by Li^+ were found to be competitive, with the disproportionation phenomenon suppressed in high concentration solutions.

ASSOCIATED CONTENT

Supporting Information. Sample Photos, experimental setup, porosity correction, calculation methods for electrical conductivity and activation energy, resonance curves of PC and PC–DME, Raman spectra and Raman data for PC-DME without $LiClO_4$.

AUTHOR INFORMATION

Corresponding Authors

Kazue Kurihara - *New Industry Creation Hatchery Center (NICHe), Tohoku University, 6-6 Aoba, Aramaki, Aoba, Sendai 980-8579, Japan*; E-mail: kazue.kurihara.b7@tohoku.ac.jp

Minoru Mizuhata - *Department of Chemical Science and Engineering, Graduate School of Engineering, Kobe University 1-1 Rokkodai-cho, Nada, Kobe 657-8501, Japan; Faculty of Chemistry, Jagiellonian University, Gronostajowa 2, 30-387 Kraków, Poland*; E-mail: mizuhata@kobe-u.ac.jp

Authors

Yoshimasa Suzuki - *Department of Chemical Science and Engineering, Graduate School of Engineering, Kobe University 1-1 Rokkodai-cho, Nada, Kobe 657-8501, Japan*

Nobuaki Kunikata - *Department of Chemical Science and Engineering, Graduate School of Engineering, Kobe University 1-1 Rokkodai-cho, Nada, Kobe 657-8501, Japan*

Motohiro Kasuya - *Institute of Multidisciplinary Research for Advanced Materials, Tohoku University, 2-1-1 Katahira, Aoba-ku, Sendai 980-8577, Japan; Faculty of Production Systems Engineering and Sciences, Komatsu University, Nu 1-3 Shicho-machi, Komatsu, Ishikawa 923-8511, Japan*

Hideshi Maki - *Department of Chemical Science and Engineering, Graduate School of Engineering, Kobe University 1-1 Rokkodai-cho, Nada, Kobe 657-8501, Japan*

Masaki Matsui - *Department of Chemical Science and Engineering, Graduate School of Engineering, Kobe University 1-1 Rokkodai-cho, Nada, Kobe 657-8501, Japan; Department of Chemistry, Faculty of Science, Hokkaido University, Kita-10 Nishi-8, Kita, Sapporo 060-0810, Japan*

‡ *Yoshimasa Suzuki and Nobuaki Kunikata contributed equally to this paper*

†† Present Addresses: Toyama Industrial Technology Research and Development Center, 383, Takaoka, Toyama 933-0981, Japan

ACKNOWLEDGMENT

The SiO_2 samples used as solid phases were kindly gifted by NIPPON AEROSIL Co. Ltd., Japan. This study is supported by the research project of No. 12101607 in “Phase Interface Science for Highly Efficient Energy Utilization” of JST Core Research for Evolutional Science and Technology (CREST). Y. S. is very grateful to the Next-Generation Outstanding Doctoral Human Development Project through Co-creation in Different Fields in the Support for Pioneering Research Initiated by the Next Generation (SPRING) of the Japan Science and Technology Agency (JST) for making his study possible by the financial support.

REFERENCES

1. Cheng, X. B.; Zhang, R.; Zhao, C. Z.; Wei, F.; Zhang, J. G.; Zhang, Q. A Review of Solid Electrolyte Interphases on Lithium Metal Anode. *Adv. Sci. (Weinh)* **2016,** *3*, 1500213. DOI: 10.1002/advs.201500213
2. Peled, E.; Menkin, S. Review-SEI: Past, Present and Future. *J. Electrochem. Soc.* **2017,** *164,* A1703–A1719. DOI: 10.1149/2.1441707jes
3. Xing, L.; Zheng, X.; Schroeder, M.; Alvarado, J.; von Wald Cresce, A.; Xu, K.; Li, Q.; Li, W. Deciphering the Ethylene Carbonate-Propylene Carbonate Mystery in Li-Ion Batteries. *Acc. Chem. Res.* **2018,** *51,* 282–289. DOI: 10.1021/acs.accounts.7b00474
4. Jurng, S.; Brown, Z. L.; Kim, J.; Lucht, B. L. Effect of Electrolyte on the Nanostructure of the Solid Electrolyte Interphase (SEI) and Performance of Lithium Metal Anodes. *Energy Environ. Sci.* **2018,** *11,* 2600–2608. DOI: 10.1039/C8EE00364E
5. Raberg, J. H.; Vatamanu, J.; Harris, S. J.; Van Oversteeg, C. H. M.; Ramos, A.; Borodin, O.; Cuk, T. Probing Electric Double-Layer Composition via In Situ Vibrational Spectroscopy and Molecular Simulations. *J. Phys. Chem. Lett.* **2019,** *10,* 3381–3389. DOI: 10.1021/acs.jpclett.9b00879
6. Pinca, J. R.; Duborg, W. G.; Jorn, R. Ion Association and Electrolyte Structure at Surface Films in Lithium-Ion Batteries. *J. Phys. Chem. C* **2021,** *125,* 7054–7066. DOI: 10.1021/acs.jpcc.1c00393

7. Abe, T.; Sagane, F.; Ohtsuka, M.; Iriyama, Y.; Ogumi, Z. Lithium-Ion Transfer at the Interface Between Lithium-Ion Conductive Ceramic Electrolyte and Liquid Electrolyte-A Key to Enhancing the Rate Capability of Lithium-Ion Batteries. *J. Electrochem. Soc.* **2005,** *152,* A2151–A2154. DOI: 10.1149/1.2042907
8. Uchida, S.; Katada, T.; Ishikawa, M. Impact of Lithium-Ion Coordination in Carbonate-Based Electrolyte on Lithium-Ion Intercalation Kinetics into Graphite Electrode. *Electrochem. Commun.* **2020,** *114*, 106705. DOI: 10.1016/j.elecom.2020.106705
9. Chapman, D. L. LI. A Contribution to the Theory of Electrocapillarity. *Philos. Mag.* **1913,** *25,* 475–481. DOI: 10.1080/14786440408634187
10. Bolt, G. H. Analysis of the Validity of the Gouy-Chapman Theory of the Electric Double Layer. *J. Colloid Sci.* **1955,** *10,* 206-218. DOI: 10.1016/0095-8522(55)90027-1
11. Verwey, E. J. W. The Electrical Double Layer and the Stability of Lyophobic Colloids. *Chem. Rev.* **1935,** *16,* 363–415. DOI: 10.1021/cr60055a002
12. Xu, K. Nonaqueous Liquid Electrolytes for Lithium-Based Rechargeable Batteries. *Chem. Rev.* **2004,** *104,* 4303–4417. DOI: 10.1021/cr030203g
13. Tarascon, J. M.; Guyomard, D. New Electrolyte Compositions Stable over the 0 to 5-V Voltage Range and Compatible with the $Li_{1+X}Mn_2O_4$/Carbon Li-Ion Cells. *Solid State Ionics* **1994,** *69,* 293–305. DOI: 10.1016/0167-2738(94)90418-9
14. Seo, D. M.; Reininger, S.; Kutcher, M.; Redmond, K.; Euler, W. B.; Lucht, B. L. Role of Mixed Solvation and Ion Pairing in the Solution Structure of Lithium Ion Battery Electrolytes. *J. Phys. Chem. C* **2015,** *119,* 14038–14046. DOI: 10.1021/acs.jpcc.5b03694
15. Mizukami, M.; Kurihara, K. Long Range Attraction Between Glass Surfaces in Cyclohexane-Ethanol Binary Liquids. *Chem. Lett.* **1999,** *28,* 1005–1006. DOI: 10.1246/cl.1999.1005
16. Mizukami, M.; Kurihara, K. Ethanol Cluster Formation on Silicon Oxide Surface in Cyclohexane–Ethanol Binary Liquids. *Chem. Lett.* **2000,** *29,* 256–257. DOI: 10.1246/cl.2000.256
17. Mizukami, M.; Moteki, M.; Kurihara, K. Hydrogen-Bonded Macrocluster Formation of Ethanol on Silica Surfaces in Cyclohexane(1). *J. Am. Chem. Soc.* **2002,** *124,* 12889–12897. DOI: 10.1021/ja027141g

18. Kitaoka, H.; Hashimoto, K.; Nishi, N.; Sakka, T. Solid Surface Induced Anisotropic Clustering in Ethanol-Cyclohexane Binary Liquids Studied by Molecular Dynamics Simulations. *Chem. Lett.* **2021,** *50,* 1662-1666. DOI: 10.1246/cl.210292
19. Matsuda, Y.; Morita, M.; Tachihara, F. Conductivity of Lithium Salts in the Mixed Systems of High Permittivity Solvents and Low Viscosity Solvents. *Bull. Chem. Soc. Jpn.* **1986,** *59,* 1967–1973. DOI: 10.1246/bcsj.59.1967
20. Suzuki, Y.; Maki, H.; Matsui, M.; Mizuhata, M. Conductivity of $LiClO_4$/PC-DME Solution Impregnated in $LiCoO_2$ Powder. *Electrochemistry* **2019,** *87,* 294–296. DOI: 10.5796/electrochemistry.19-00044
21. Smith, G. D.; Borodin, O.; Russo, S. P.; Rees, R. J.; Hollenkamp, A. F. A Molecular Dynamics Simulation Study of $LiFePO_4$/Electrolyte Interfaces: Structure and Li^+ Transport in Carbonate and Ionic Liquid Electrolytes. *Phys. Chem. Chem. Phys.* **2009,** *11,* 9884–9897. DOI: 10.1039/b912820d
22. Vatamanu, J.; Borodin, O.; Smith, G. D. Molecular Dynamics Simulation Studies of the Structure of a Mixed Carbonate/$LiPF_6$ Electrolyte near Graphite Surface as a Function of Electrode Potential. *J. Phys. Chem. C* **2012,** *116,* 1114–1121. DOI: 10.1021/jp2101539
23. Xing, L.; Vatamanu, J.; Borodin, O.; Smith, G. D.; Bedrov, D. Electrode/Electrolyte Interface in Sulfolane-Based Electrolytes for Li Ion Batteries: A Molecular Dynamics Simulation Study. *J. Phys. Chem. C* **2012,** *116,* 23871–23881. DOI: 10.1021/jp3054179
24. Boyer, M. J.; Vilčiauskas, L.; Hwang, G. S. Structure and Li^+ Ion Transport in a Mixed Carbonate/$LiPF_6$ Electrolyte near Graphite Electrode Surfaces: A Molecular Dynamics Study. *Phys. Chem. Chem. Phys.* **2016,** *18,* 27868–27876. DOI: 10.1039/c6cp05140e
25. Steinrück, H. G.; Cao, C.; Tsao, Y.; Takacs, C. J.; Konovalov, O.; Vatamanu, J.; Borodin, O.; Toney, M. F. The Nanoscale Structure of the Electrolyte–Metal Oxide Interface. *Energy Environ. Sci.* **2018,** *11,* 594–602. DOI: 10.1039/C7EE02724A
26. Yu, L.; Liu, H.; Wang, Y.; Kuwata, N.; Osawa, M.; Kawamura, J.; Ye, S. Preferential Adsorption of Solvents on the Cathode Surface of Lithium Ion Batteries. *Angew. Chem. Int. Ed. Engl.* **2013,** *52,* 5753–5756. DOI: 10.1002/anie.201209976
27. Peng, Q.; Liu, H.; Ye, S. Adsorption of Organic Carbonate Solvents on a Carbon Surface Probed by Sum Frequency Generation (SFG) Vibrational Spectroscopy. *J. Electroanal. Chem.* **2017,** *800,* 134–143. DOI: 10.1016/j.jelechem.2016.09.006

28. Mizukami, M.; Kurihara, K. A New Physical Model for Resonance Shear Measurement of Confined Liquids Between Solid Surfaces. *Rev. Sci. Instrum.* **2008,** *79*, 113705. DOI: 10.1063/1.3012811
29. Kasuya, M.; Kurihara, K. Novel Surface Forces Apparatus for Characterizing Solid–Liquid Interfaces. *Electrochemistry* **2014,** *82,* 317–321. DOI: 10.5796/electrochemistry.82.317
30. Grunberg, B.; Emmler, T.; Gedat, E.; Shenderovich, I.; Findenegg, G. H.; Limbach, H. H.; Buntkowsky, G. Hydrogen Bonding of Water Confined in Mesoporous Silica MCM-41 and SBA-15 Studied by ^{1}H Solid-State NMR. *Chem.─Eur. J.* **2004,** *10,* 5689– 5696. DOI: 10.1002/chem.200400351
31. Maki, H.; Sogawa, R.; Fukui, M.; Deki, S.; Mizuhata, M. Quantitative Analysis of Water Activity Related to Hydration Structure in Highly Concentrated Aqueous Electrolyte Solutions. *Electrochemistry* **2019,** *87,* 139–141. DOI: 10.5796/electrochemistry.18-00087
32. Maki, H.; Takemoto, M.; Sogawa, R.; Mizuhata, M. Solvent Molecule Mobilities in Propylene Carbonate-Based Electrolyte Solutions Coexisting with Fumed Oxide Nanoparticles. *Colloids Surf. A Physicochem. Eng. Aspects* **2019,** *562,* 270–279. DOI: 10.1016/j.colsurfa.2018.11.045
33. Maki, H.; Tachibana, T.; Eun, S. J.; Mizuhata, M. Estimation of Solid–Liquid Interfacial Potential Enabled by Quantitative Analysis and Relaxation Observation of Quadrupolar NMR. *Colloids Surf. A Physicochem. Eng. Aspects* **2020,** *604*. DOI: 10.1016/j.colsurfa.2020.125286
34. Kasuya, M.; Hino, M.; Yamada, H.; Mizukami, M.; Mori, H.; Kajita, S.; Ohmori, T.; Suzuki, A.; Kurihara, K. Characterization of Water Confined Between Silica Surfaces Using the Resonance Shear Measurement. *J. Phys. Chem. C* **2013,** *117,* 13540–13546. DOI: 10.1021/jp404378b
35. Ueno, K.; Kasuya, M.; Watanabe, M.; Mizukami, M.; Kurihara, K. Resonance Shear Measurement of Nanoconfined Ionic Liquids. *Phys. Chem. Chem. Phys.* **2010,** *12,* 4066–4071. DOI: 10.1039/b923571j
36. Yamada, Y.; Furukawa, K.; Sodeyama, K.; Kikuchi, K.; Yaegashi, M.; Tateyama, Y.; Yamada, A. Unusual Stability of Acetonitrile-Based Superconcentrated Electrolytes for Fast-Charging Lithium-Ion Batteries. *J. Am. Chem. Soc.* **2014,** *136,* 5039–5046. DOI: 10.1021/ja412807w
37. Suo, L.; Borodin, O.; Gao, T.; Olguin, M.; Ho, J.; Fan, X.; Luo, C.; Wang, C.; Xu, K. Water-in-Salt. *Science* **2015,** *350,* 938–943. DOI: 10.1126/science. aab1595

38. Miyazaki, K.; Shimada, T.; Ito, S.; Yokoyama, Y.; Fukutsuka, T.; Abe, T. Enhanced Resistance to Oxidative Decomposition of Aqueous Electrolytes for Aqueous Lithium-Ion Batteries. *Chem. Commun. (Camb)* **2016,** *52,* 4979–4982. DOI: 10.1039/c6cc00873a
39. Yokoyama, Y.; Fukutsuka, T.; Miyazaki, K.; Abe, T. Origin of the Electrochemical Stability of Aqueous Concentrated Electrolyte Solutions. *J. Electrochem. Soc.* **2018,** *165,* A3299–A3303. DOI: 10.1149/2.0491814jes
40. Wang, L.; Uosaki, K.; Noguchi, H. Effect of Electrolyte Concentration on the Solvation Structure of Gold/LITFSI–DMSO Solution Interface. *J. Phys. Chem. C* **2020,** *124,* 12381–12389. DOI: 10.1021/acs.jpcc.0c00827
41. Wang, M.; Huai, L.; Hu, G.; Yang, S.; Ren, F.; Wang, S.; Zhang, Z.; Chen, Z.; Peng, Z.; Shen, C.; Wang, D. Effect of LiFSI Concentrations to Form Thickness- and Modulus-Controlled SEI Layers on Lithium Metal Anodes. *J. Phys. Chem. C* **2018,** *122,* 9825–9834. DOI: 10.1021/acs.jpcc.8b02314
42. Lahiri, A.; Pulletikurthi, G.; Shapouri Ghazvini, M. S.; Höfft, O.; Li, G.; Endres, F. Ionic Liquid-Organic Solvent Mixture-Based Polymer Gel Electrolyte with High Lithium Concentration for Li-Ion Batteries. *J. Phys. Chem. C* **2018,** *122,* 24788–24800. DOI: 10.1021/acs.jpcc.8b07745
43. Horn, R. G.; Smith, D. T.; Haller, W. Surface Forces and Viscosity of Water Measured Between Silica Sheets. *Chem. Phys. Lett.* **1989,** *162,* 404–408. DOI: 10.1016/0009-2614(89)87066-6
44. Ren, H. Y.; Mizukami, M.; Kurihara, K. Preparation of Stable Silica Surfaces for Surface Forces Measurement. *Rev. Sci. Instrum.* **2017,** *88*, 095108. DOI: 10.1063/1.4986613
45. Israelachvili, J. N. Thin Film Studies Using Multiple-Beam Interferometry. *J. Colloid Interface Sci.* **1973,** *44,* 259–272. DOI: 10.1016/0021-9797(73)90218-X
46. Horn, R. G.; Smith, D. T. Analytic Solution for the Three-Layer Multiple Beam Interferometer. *Appl. Opt.* **1991,** *30,* 59–65. DOI: 10.1364/AO.30.000059
47. Mizuhata, M.; Cha, G.; Harada, Y.; Kimura, H.; Kajinami, A.; Deki, S. Electrical Conductivity of Lithium Electrolyte Solution in Hetero-Phase Systems. *Proc. Electrochem. Soc.* **2000,** *99–25,* 463–470.

48. Matsuda, Y.; Nakashima, H.; Morita, M.; Takasu, Y. Behavior of Some Ions in Mixed Organic Electrolytes of High Energy Density Batteries. *J. Electrochem. Soc.* **1981,** *128,* 2552–2556. DOI: 10.1149/1.2127289
49. Matsuda, Y.; Morita, M.; Kosaka, K. Conductivity of the Mixed Organic Electrolyte Containing Propylene Carbonate and 1,2-Dimethoxyethane. *J. Electrochem. Soc.* **1983,** *130,* 101–104. DOI: 10.1149/1.2119630
50. Battisti, D.; Nazri, G. A.; Klassen, B.; Aroca, R. Vibrational Studies of Lithium Perchlorate in Propylene Carbonate Solutions. *J. Phys. Chem.* **1993,** *97,* 5826–5830. DOI: 10.1021/j100124a007
51. Sagane, F.; Abe, T.; Ogumi, Z. Li^+-Ion Transfer Through the Interface Between Li^+-Ion Conductive Ceramic Electrolyte and Li^+-Ion-Concentrated Propylene Carbonate Solution. *J. Phys. Chem. C* **2009,** *113,* 20135–20138. DOI: 10.1021/jp908623c
52. Fukushima, K.; Chibahara, H. Conformational Difference Due to Types of Cation in 1,2-Dimethoxyethane-Cation Complexes as Studied by Raman and FT-IR Spectroscopy. *J. Mol. Struct.* **1993,** *291,* 145–150. DOI: 10.1016/0022-2860(93)85038-V
53. Yoshida, H.; Matsuura, H. Density Functional Study of the Conformations and Vibrations of 1,2-Dimethoxyethane. *J. Phys. Chem. A* **1998,** *102,* 2691–2699. DOI: 10.1021/jp9800766
54. Yoshi, M.; Holzleithner, K.; Isono, K.; Nakamurra, H. Selective Solvation Towards Lithium in Non-Aqueous Solvents. *Denki Kagaku* **1988,** *56,* 662–663.
55. Atkins, P.; Hefter, G. T.; Singh, P. Ion Solvation in Lithium Battery Electrolyte Solutions Part II. Solvent Effects on Lithium-Ion Intercalation in Niobium Triselenide. *J. Power Sources* **1991,** *36,* 17–27. DOI: 10.1016/0378-7753(91)80041-U
56. Yoshio, M.; Nakamura, H.; Hyakutake, M.; Nishikawa, S.; Yoshizuka, K. Conductivities of 1,2-Dimethoxyethane or 1,2-Dimethoxyethane-Related Solutions of Lithium Salts. *J. Power Sources* **1993,** *41,* 77–86. DOI: 10.1016/0378-7753(93)85006-A
57. Fukushima, T.; Matsuda, Y.; Hashimoto, H.; Arakawa, R. Solvation of Lithium Ions in Organic Electrolytes of Primary Lithium Batteries by Electrospray Ionization-Mass Spectroscopy. *J. Power Sources* **2002,** *110,* 34–37. DOI: 10.1016/S0378-7753(02)00168-4
58. Postupna, O. O.; Kolesnik, Y. V.; Kalugin, O. N.; Prezhdo, O. V. Microscopic Structure and Dynamics of $LiBF_4$ Solutions in Cyclic and Linear Carbonates. *J. Phys. Chem. B* **2011,** *115,* 14563–14571. DOI: 10.1021/jp206006m

59. Chaban, V. Solvation of Lithium Ion in Dimethoxyethane and Propylene Carbonate. *Chem. Phys. Lett.* **2015,** 631, 1– 5 DOI: 10.1016/j.cplett.2015.04.047
60. Gutmann, V. Empirical parameters for donor and acceptor properties of solvents. *Electrochim. Acta* **1976,** 21, 661-670 DOI: 10.1016/0013-4686(76)85034-7

For Table of Contents Graphic

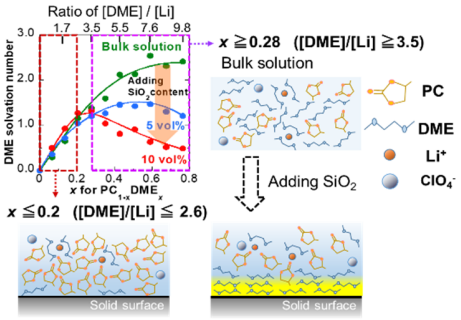

Supporting Information for：

Disproportionation Phenomenon at the Silica Interface of Propylene Carbonate–1,2-Dimethoxyethane Binary Solvent containing Lithium Perchlorate

Yoshimasa Suzuki, [†, ‡] *Nobuaki Kunikata,* [†, ‡, ††] *Motohiro Kasuya,* [¶, ||] *Hideshi Maki,* [†] *Masaki Matsui,* [†, #] *Kazue Kurihara,* [Δ,] * *and Minoru Mizuhata*[†, §,] *

[†]Department of Chemical Science and Engineering, Graduate School of Engineering, Kobe University, 1-1 Rokkodai-cho, Nada, Kobe 657-8501, Japan

[¶]Institute of Multidisciplinary Research for Advanced Materials, Tohoku University, 2-1-1 Katahira, Aoba-ku, Sendai 980-8577, Japan

[||]Faculty of Production Systems Engineering and Sciences, Komatsu University, Nu 1-3 Shicho-machi, Komatsu, Ishikawa 923-8511, Japan

[#]Department of Chemistry, Faculty of Science, Hokkaido University, Kita-10 Nishi-8, Kita, Sapporo 060-0810, Japan

[Δ]New Industry Creation Hatchery Center (NICHe), Tohoku University, 6-6 Aoba, Aramaki, Aoba, Sendai 980-8579, Japan

[§]Faculty of Chemistry, Jagiellonian University, Gronostajowa 2, 30-387 Kraków, Poland

E-mail: mizuhata@kobe-u.ac.jp

Phone: +81-78-803-6186

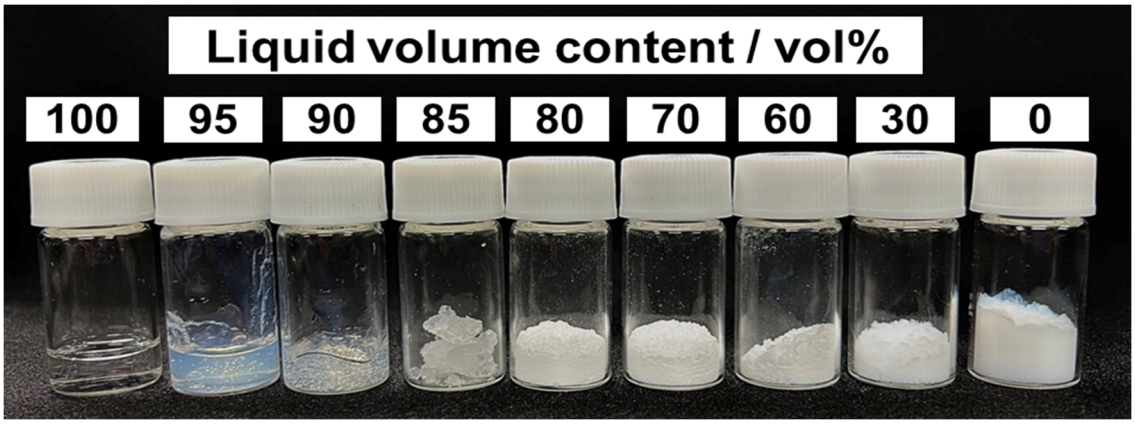

Figure S1. Photographs of $SiO_2/PC_{0.5}DME_{0.5}$ samples mixed at each liquid phase volume fraction.

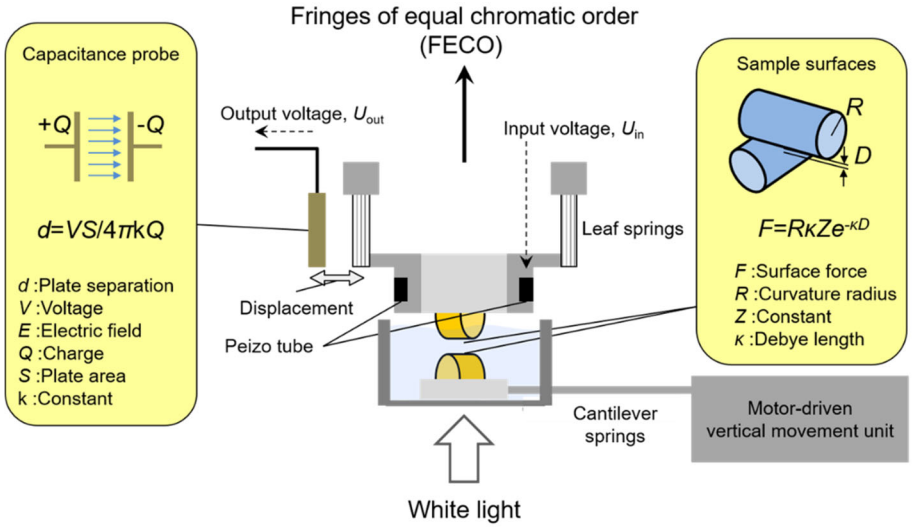

Figure S2. Schematic representation of experimental setups of resonance shear measurement (RSM).

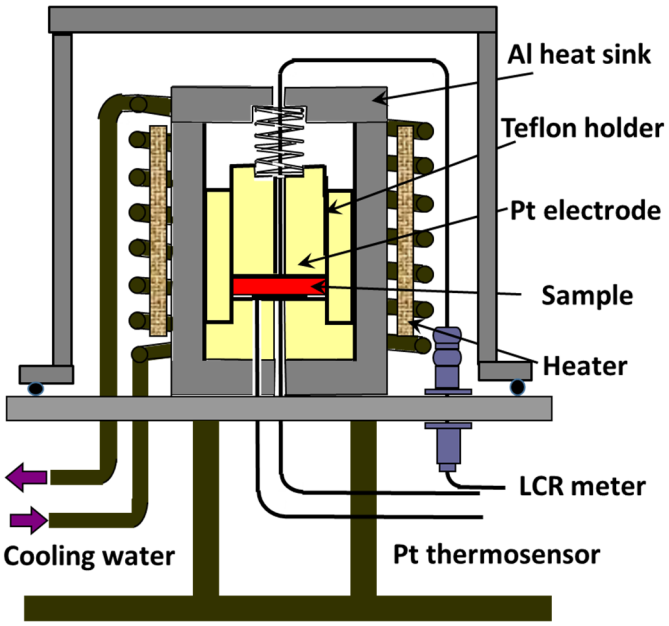

Figure S3. Schematic representation of experimental setups of AC impedance measurement.

How to consider pore volume in q-^{1}HNMR measurement

In NMR measurements, the intensity is detected according to the number of nuclides contained in the volume irradiated with the magnetic field. Therefore, when quantitatively measuring a sample of a solid-liquid coexistence system, it is necessary to accurately estimate the volume of the liquid phase contained in each unit volume. What is important is the existence of pore volume (V_p). V_p is the volume that is not filled with the electrolyte in the gap that exists when the solid powder is filled. For this evaluation, we decided to estimate the pore volume from the ratio of the true density of SiO_2 to the tap density, as shown in Fig. S3. In this sample, the true density (d) was 1.98 g cm^{-3} and the tap density (d_b) was 0.91 g cm^{-3}. Therefore, the porosity when filled with powder is 45.8 vol%. Therefore, when the liquid phase volume fraction ($\emptyset_L$) is 45.8 vol% or less, the gap cannot be filled with the liquid phase, so there is a pore volume (V_p). From the above, it is considered that the amount detected by ^{1}H NMR can be expressed by the following formula.

$$\frac{I_{\text{sample}}}{I_{\text{bulk liquid}}} = \frac{V_L}{V_L + V_s + V_p}$$

Where V_L is the volume of the liquid phase, V_S is the volume of the solid phase, and V_p is the pore volume. However, when $\emptyset_L$ is 45.8 vol% or more, V_p = 0. Therefore, the dashed line showing the amount detected by ^{1}H NMR in Figure 2. (a)-(c) bends when $\emptyset_L$ is 45.8 vol% or less.

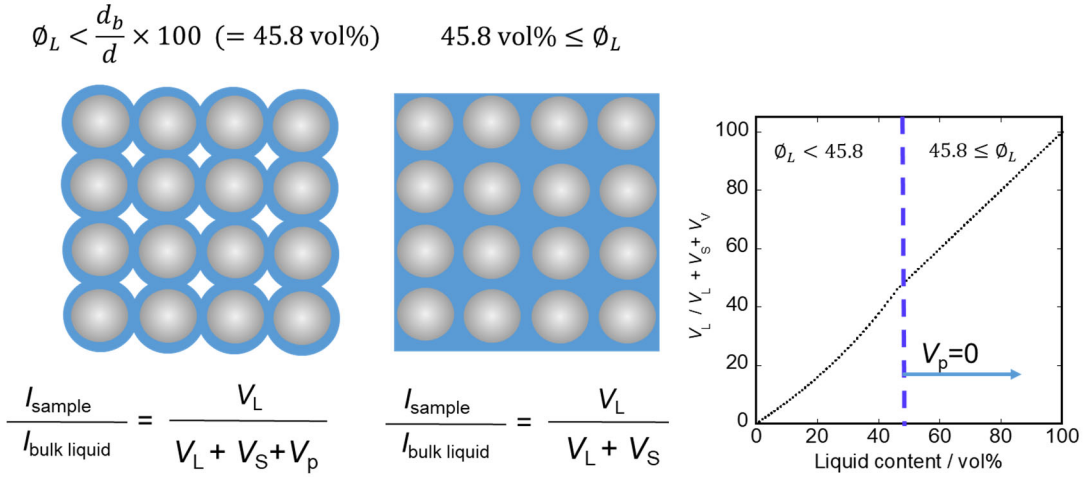

Figure S4. Detected amount of ^{1}H-qNMR expected from liquid content of solid-liquid coexisting sample. Corresponds to the broken line in Figure 2. (a)-(c) and Figure 7 (a),(c).

How to calculate the thickness of the DME layer not detected by ^{1}H NMR measurement.

The thickness of the DME layer, which was not detected by ^{1}H NMR measurements, was calculated using the apparent average thickness (l) defined in Equation 1 in the text, using the following formula.
Thickness of DME layer not detected by ^{1}H NMR = 0.45l ×undetected ration of DME
0.45 is the volume ratio of DME in $PC_{0.6}DME_{0.4}$. The undetected rate of DME was calculated from the ratio of the actual amount detected to the amount originally detected by ^{1}H NMR, indicated by the dashed line in Figure S4. Table S1 shows the distances not detected by ^{1}H NMR for each liquid phase volume fraction in $SiO_2/PC_{0.6}DME_{0.4}$.

Table S1. DME layer thickening not detected by ^{1}H NMR measurements at each liquid phase volume fraction in $SiO_2/PC_{0.6}DME_{0.4}$.

Volume fraction of liquid phase / vol%	Thickness of DME layer not detected by ^{1}H NMR / nm
90	3.40
80	1.86
70	1.32
60	0.93
50	0.78
40	0.53
30	0.36
22.5	0.26
20	0.95

Calculation method of electric conductivity

Fig. S5 (a) shows the Nyquist plot obtained by impedance measurement of SiO_2 / 1.0 mol L^{-1} $LiClO_4$ PC and Fig. S5 (b) shows the Nyquist plot of SiO_2 / 1.0 mol L^{-1} $LiClO_4$ $PC_{0.55}DME_{0.45}$. Except for the SiO_2 / 1.0 mol L^{-1} $LiClO_4$ $PC_{0.55}DME_{0.45}$ sample, which has a liquid phase volume fraction of 15 vol%, a semicircular part appears on the high frequency side and a straight part appears on the low frequency side, and the diameter of the semicircle increased as the liquid phase amount decreased. In the sample of SiO_2 / 1.0 mol L^{-1} $LiClO_4$ $PC_{0.55}DME_{0.45}$, the resistance value is too large, so it is considered that the measured value on the low frequency side is disturbed. We concluded that the electrical conduction path does not change in each sample, and since SiO_2 is an insulator, the diameter of the semicircle is regarded as the resistance value of ion conduction in the solution in a solid-liquid coexistence system.

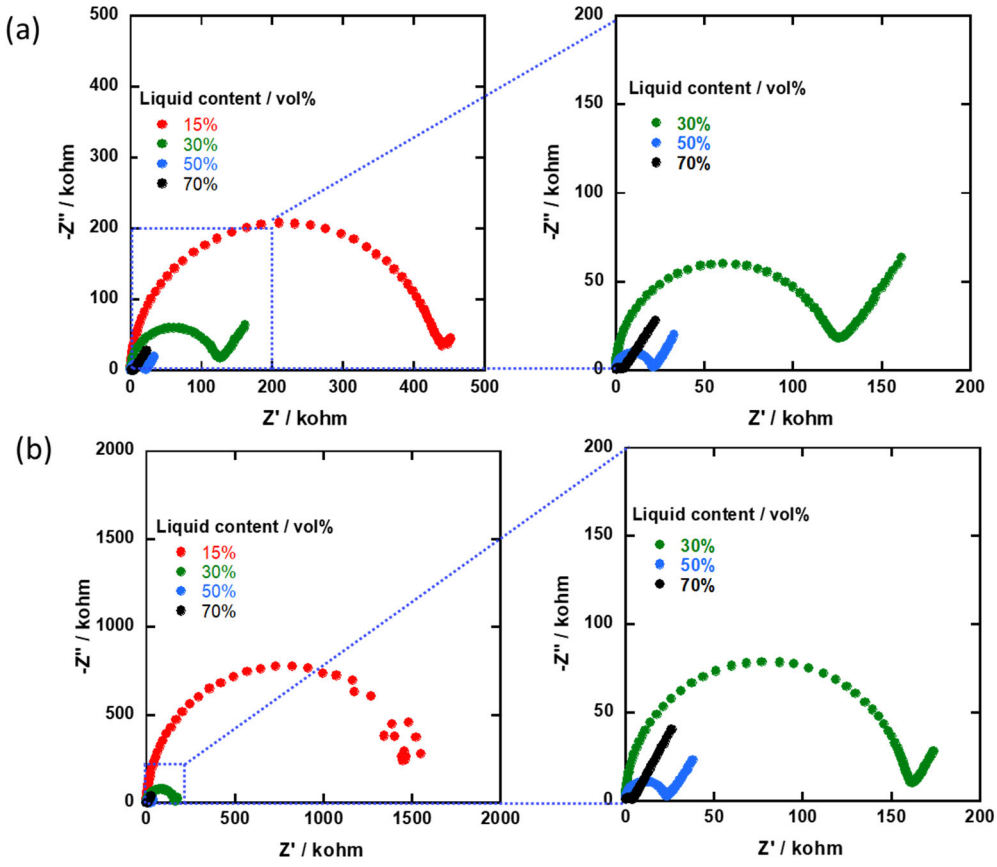

Figure S5. Nyquist plot obtained by impedance measurement of (a) SiO_2 / 1mol L^{-1} $LiClO_4$ PC, (b) SiO_2 / 1mol L^{-1} $LiClO_4$ $PC_{0.55}DME_{0.45}$.

Calculation method of activation energy

Figure. S5 shows some examples of the temperature dependence of electrical conductivity. From these temperature dependences, the activation energy was calculated by the Arrhenius plot or the VTF plot.

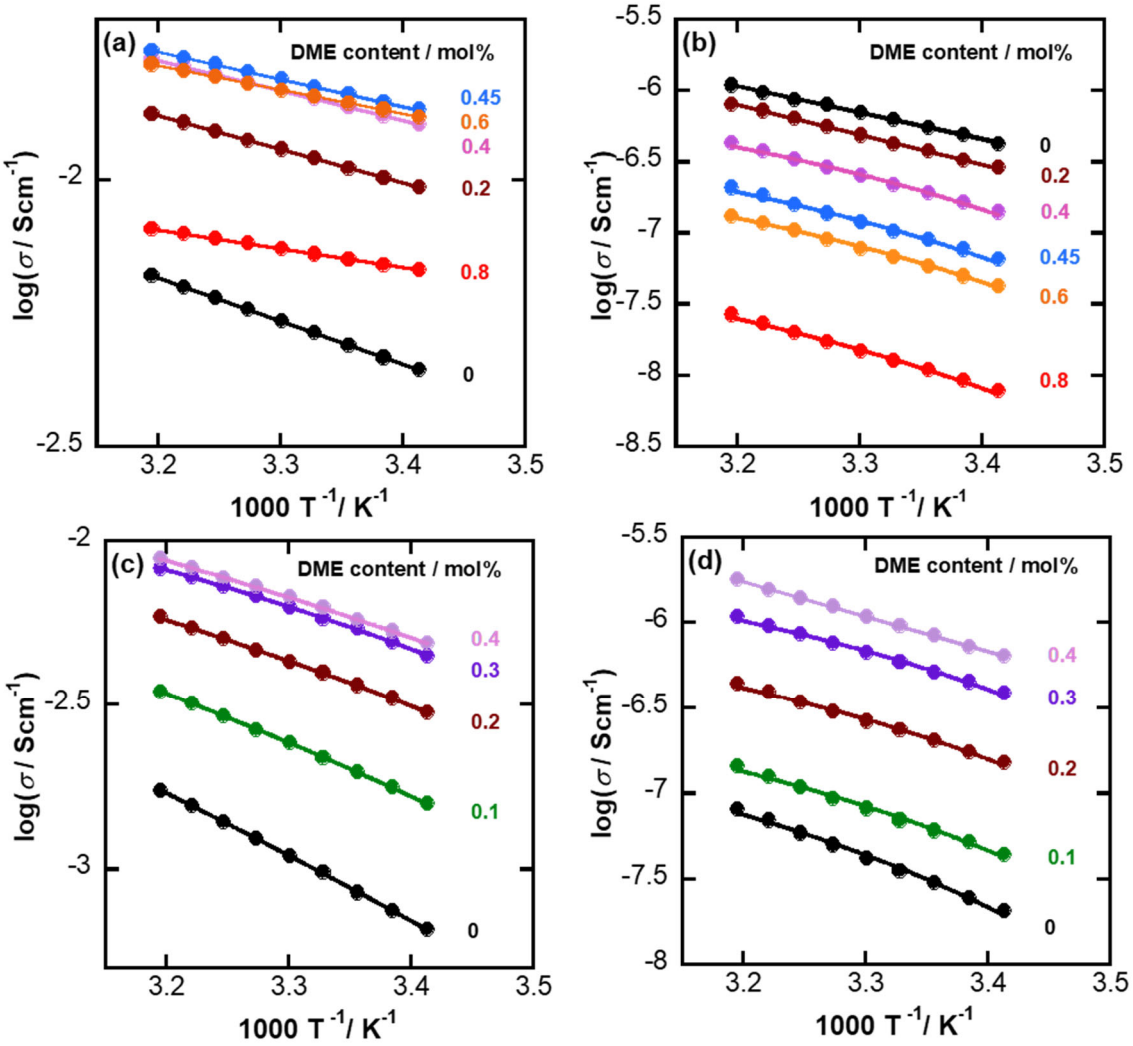

Figure S6. Temperature dependence of conductivity at each DME content for (a) 1.0 molL^{-1} $LiClO_4$-$PC_{1-x}DME_x$ solution, (b) SiO_2 / 1.0 mol L^{-1} $LiClO_4$ -$PC_{1-x}DME_x$ solution coexisting systems, (c) 3.0 mol L^{-1} $LiClO_4$-$PC_{1-x}DME_x$ solution, (d) SiO_2 / 3.0 mol L^{-1} $LiClO_4$ -$PC_{1-x}DME_x$ solution coexisting systems. Liquid content: φ =15 vol% for (b) and (d).

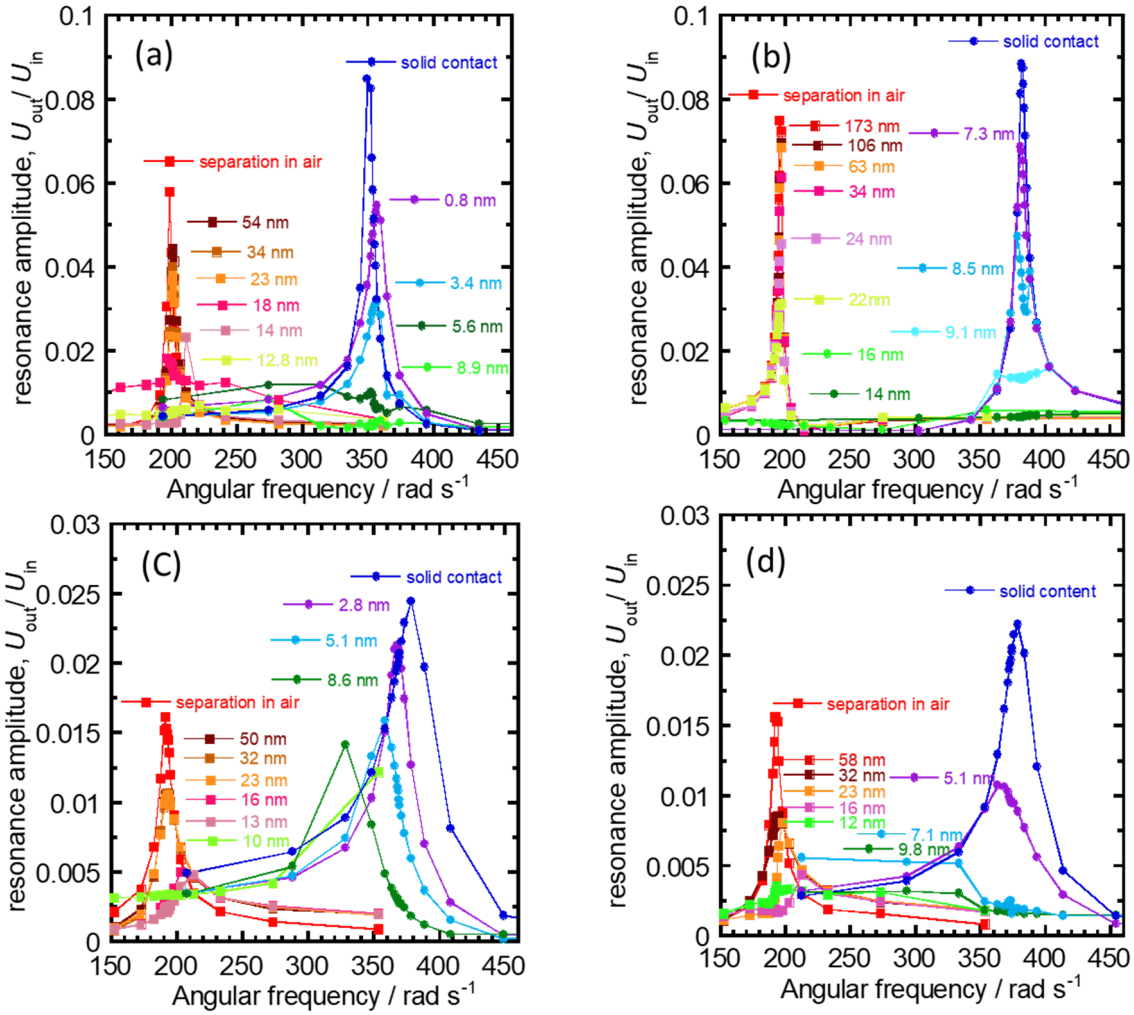

Figure S7. Resonance curves of (a)PC, (b) 1.0 mol L^{-1} PC, (c) 2.0 mol L^{-1} PC, (d) 3.0 mol L^{-1} PC confined between sputtered silica surfaces at various surface separations.

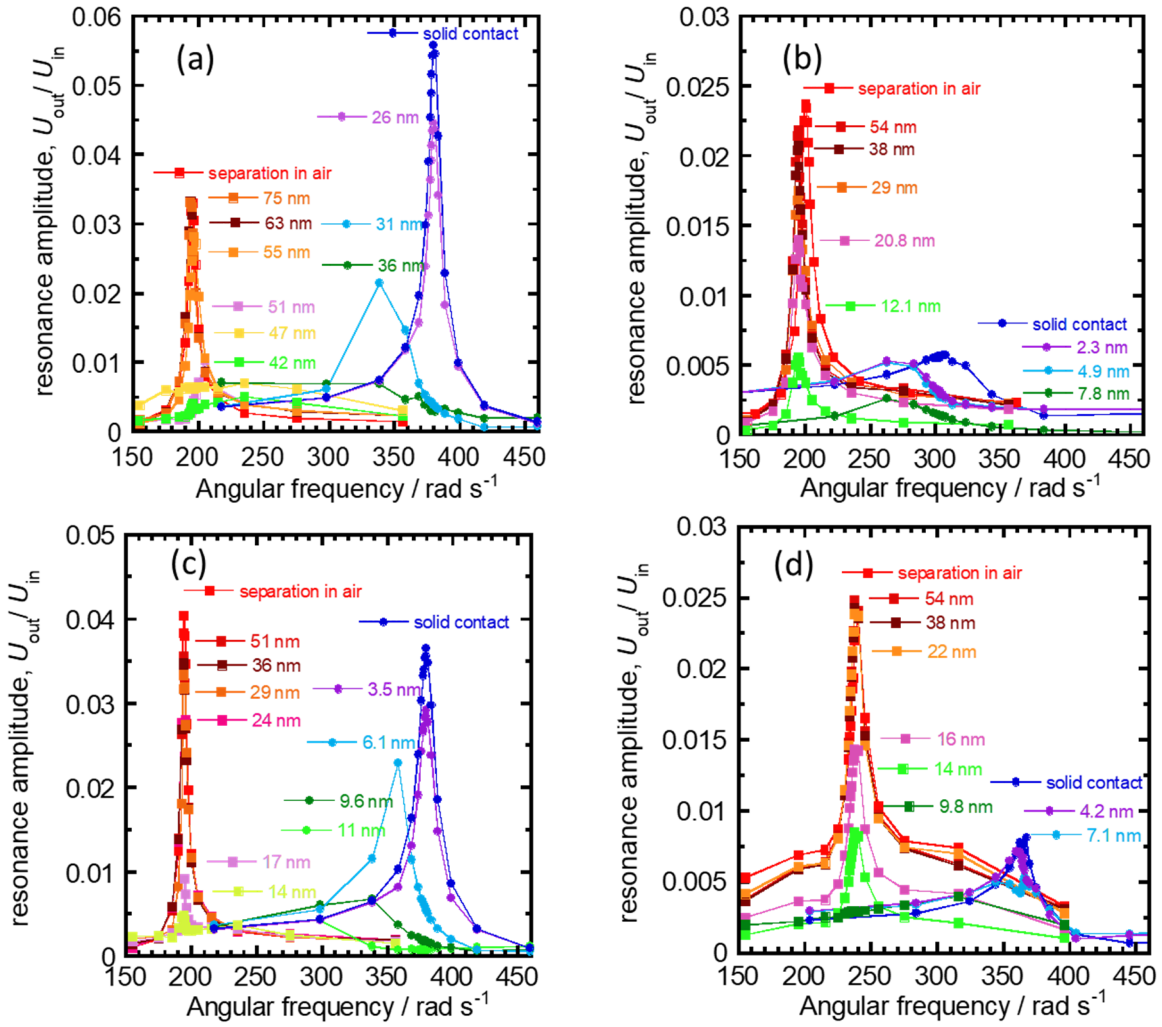

Figure S8. Resonance curves of (a) $PC_{0.6}DME_{0.4}$, (b) 1.0 mol L^{-1} $PC_{0.6}DME_{0.4}$, (c) 2.0 mol L^{-1} $PC_{0.6}DME_{0.4}$ (d) 3.0 mol L^{-1} $PC_{0.6}DME_{0.4}$ confined between sputtered silica surfaces at various surface separations.

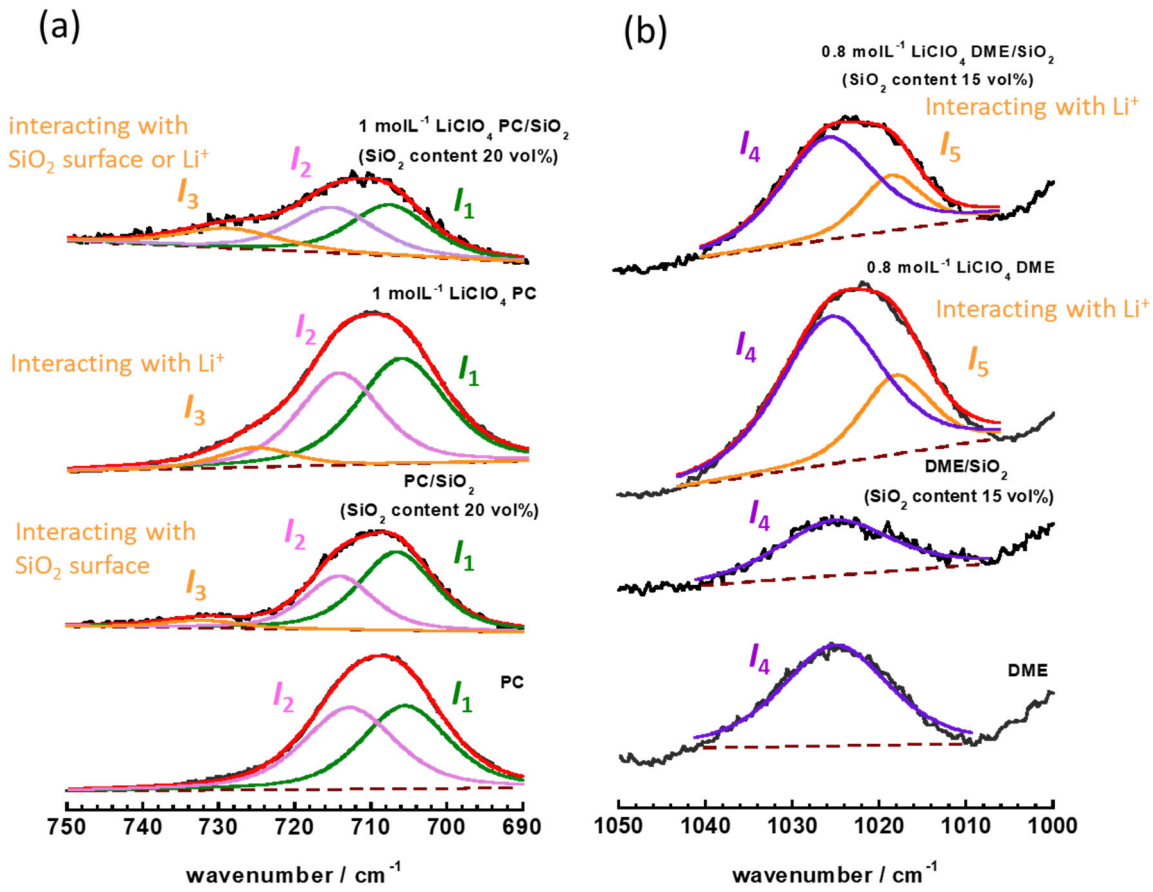

Figure S9. Raman spectra (a) of symmetrical symmetry ring deformation band of PC (b) of C-O-C stretching vibration band of DME.

I_1 is assigned to free PC without interactions (707 cm^{-1}). I_2 is assigned to PC with intermolecular interactions (714 cm^{-1}). I_3 is assigned to PC interacting with the SiO_2 surface and PC solvated with Li^+ (730 cm^{-1}). I_4 is assigned to free DME (1025 cm^{-1}). I_5 is assigned to DME solvated with Li^+ (1017 cm^{-1}).

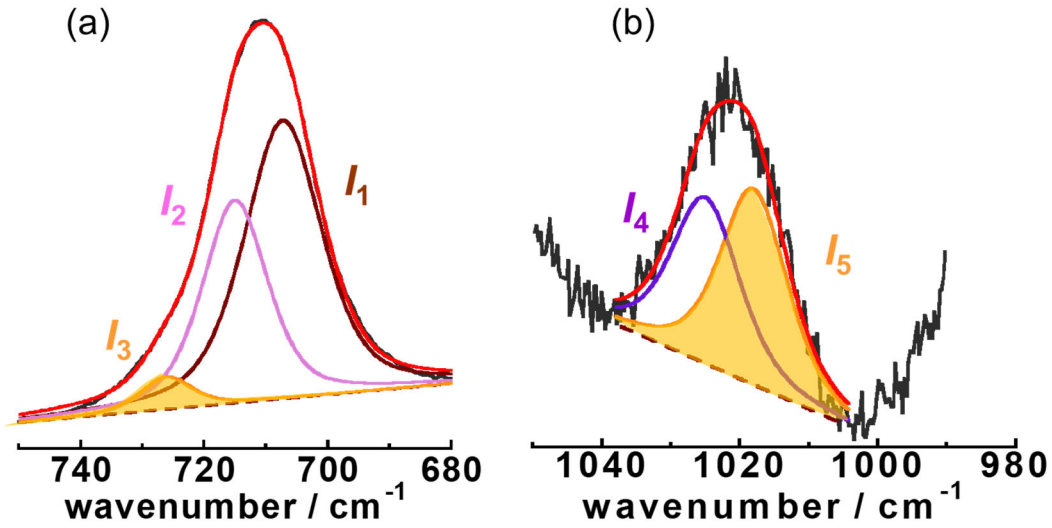

Figure S10. Raman spectra (a) of symmetrical symmetry ring deformation band of PC and (b) of C-O-C stretching vibration band of DME for for 1.0 mol L^{-1} $LiClO_4$ $PC_{0.8}DME_{0.2}$ (Liquid content 90 vol%).

I_1 is assigned to free PC without interactions (707 cm^{-1}). I_2 is assigned to PC with intermolecular interactions (714 cm^{-1}). I_3 is assigned to PC interacting with the SiO_2 surface and PC solvated with Li^+ (730 cm^{-1}).

I_4 is assigned to free DME (1025 cm^{-1}). I_5 is assigned to DME solvated with Li^+ (1017 cm^{-1}).

A discussion of Raman data for PC-DME without $LiClO_4$

Figure S10 shows the dependence of the relative intensity of I_3 or I_5 on the DME content for SiO_2/ $PC_{1-x}DME_x$. Because they do not contain $LiClO_4$, I_3 is the peak of PC interacting with the SiO_2 surface. From Figure S10(a), it is clear that the relative intensity of I_3 decreases with increasing DME content, indicating a decrease in PCs interacting with the SiO_2 surface. This result supports the phenomenon that DME preferentially interacts with SiO_2 surfaces. From Figure S10(b), the C-O-C stretching vibration peak of DME appears only in I_4 for all DME compositions, and the I_5 peak is observed only when solvated with Li^+, regardless of the presence of SiO_2 or PC, confirming that the I_5 peak is that of DME solvated with Li^+.

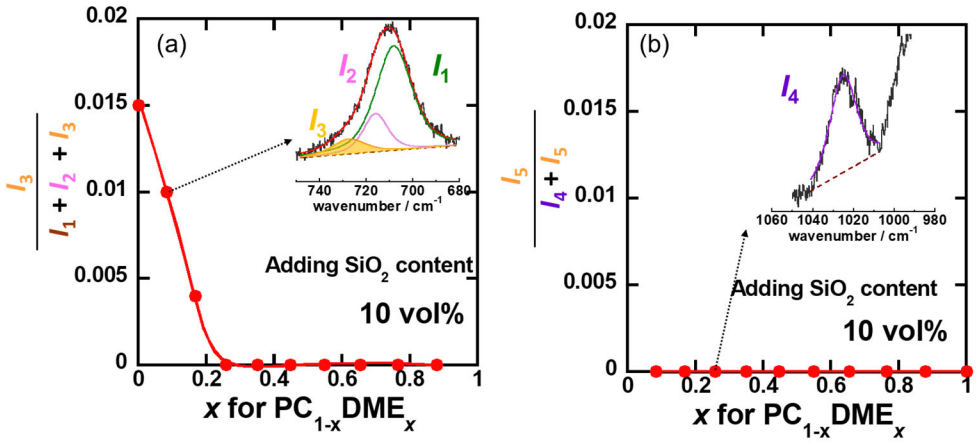

Figure S11. (a) Dependence of the relative intensity of I_3 on the DME content for $SiO_2/PC_{1-x}DME_x$ at 90 vol% liquid contents. I_1 is assigned to free PC without interactions (707 cm^{-1}). I_2 is assigned to PC with intermolecular interactions (714 cm^{-1}). I_3 is assigned to PC interacting with the SiO_2 surface (730 cm^{-1}). Inset shows Raman spectra of symmetry ring deformation bands of PC in $SiO_2/PC_{0.92}DME_{0.08}$ (Liquid content: 10 vol%) (b) Dependence of the relative intensity of I_5 and (b) the solvation number of DME on DME content for $SiO_2/PC_{1-x}DME_x$ at 90 vol% liquid contents. I_4 is assigned to free DME (1025 cm^{-1}). I_5 is assigned to DME solvated with Li^+ (1017 cm^{-1}). Inset shows Raman spectra of C-O-C stretching vibration band of DME in $SiO_2/PC_{0.74}DME_{0.26}$ (Liquid content: 10 vol%).